Reactivity of Terminal, Electrophilic Phosphinidene Complexes of Molybdenum and Tungsten. Nucleophilic Addition at Phosphorus and P−P Bond Forming Reactions with Phosphines and Diphosphines

Brian T. Sterenberg,*[,†,‡] Ozan Sanli Senturk,[‡,§] Konstantin A. Udachin,[‡] and Arthur J. Carty*[,‡]

Steacie Institute for Molecular Sciences, National Research Council of Canada, 100 Sussex Drive, Ottawa, Ontario, Canada K1A 0R6, and Department of Chemistry and Biochemistry, University of Regina, 3737 Wascana Parkway, Regina, Saskatchewan, Canada S4S 0A2

Received July 31, 2006

Reaction of the terminal electrophilic phosphinidene complexes $[Cp^*M(CO)_3\{PN(i\text{-}Pr)_2\}][AlCl_4]$ (**3**, M = Mo; **4**, M = W) with PEt_3 results in replacement of a metal carbonyl by the phosphine. The reactions occur via initial nucleophilic attack by the phosphine at the phosphinidene phosphorus, followed by carbonyl loss and migration of the phosphine to the metal. Reactions of **3** and **4** with bis(dimethylphosphino)methane (dmpm) lead to $[Cp^*M(CO)_2\{P(N(i\text{-}Pr)_2)P(Me_2)CH_2P(Me_2)\text{-}\kappa^2P^1,P^4\}][AlCl_4]$ (**9**, M = Mo; **10**, M = W), in which one end of the diphosphine coordinates to phosphorus and the other end coordinates to the metal. The reactions proceed by initial nucleophilic attack by one end of the diphosphine at phosphorus, followed by carbonyl loss and coordination of the other end of the ligand to the metal. Compound **3** (M = Mo) reacts with bis(dimethylphosphino)ethane (dmpe) to give the analogous product $[Cp^*Mo(CO)_2\{P(N(i\text{-}Pr)_2)P(Me_2)CH_2CH_2P(Me_2)\text{-}\kappa^2P^1,P^5\}][AlCl_4]$ (**12**), in which the two ends of the dmpe ligand coordinate to phosphorus and molybdenum, respectively. Reaction of compound **4** (M = W) with dmpe leads to two products, $[Cp^*W(CO)_2\{P(N(i\text{-}Pr)_2)P(Me_2)CH_2CH_2P(Me_2)\text{-}\kappa^2P^1,P^5\}][AlCl_4]$ (**13**) and $[\{Cp^*W(CO)_2(PN(i\text{-}Pr)_2)\}_2(\mu\text{-dmpe})][AlCl_4]_2$ (**14**). Compound **13** is analogous to **12**. In compound **14**, the two ends of the diphosphine ligand displace carbonyl ligands from two molecules of **4**, resulting in a novel bis-phosphinidene structure in which the diphosphine ligand bridges two metal centers, each of which retains a terminal phosphinidene ligand. Loss of an additional carbonyl ligand from **12**, followed by migration of one end of the phosphine from phosphorus to the metal, results in re-formation of a terminal phosphinidene ligand, leading to $[Cp^*Mo(CO)(PN(i\text{-}Pr)_2)(dmpe\text{-}\kappa^2P)][AlCl_4]$ (**17**). The structural characterization of the phosphine adducts and carbonyl substitution products of the terminal phosphinidene complexes **3** and **4** has provided valuable insights into metal−phosphinidene bonding in these compounds.

Introduction

Transition-metal phosphinidene complexes can be considered analogues of carbene complexes. It has thus been suggested that, like carbenes, they can be divided into nucleophilic and electrophilic classes.[1−4] The first stable nucleophilic terminal phosphinidene complexes were described by Lappert in 1987,[5] and other nucleophilic phosphinidene complexes, analogous to Schrock type carbenes, have been described since.[6] The isolation of electrophilic phosphinidene complexes has proven to be more difficult.[4,7] However, extensive studies of transient electrophilic phosphinidene complexes have been carried out.[3,8] In particular, the transient molecules $[W(CO)_5PR]$, generated via thermal decomposition of phosphanorbornadiene complexes in the presence of trapping reagents, have been used to explore many different reactions of the phosphinidene fragment.[9] These trapping reactions, in conjunction with computational studies,[1,2,10,11] form much of the basis for our understanding of the reactivity of electrophilic phosphinidenes.

In 2001, we reported the synthesis of stable terminal electrophilic phosphinidene complexes of molybdenum, tungsten, and ruthenium.[12,13] These were the first examples of a new class of cationic phosphinidene complexes formed by abstraction of chloride from terminal chloro−phosphido complexes. Since then, the number of known stable phosphinidene complexes has

* To whom correspondence should be addressed. E-mail: brian.sterenberg@uregina.ca (B.T.S.); acarty@pco-bcp.gc.ca (A.J.C.).

† University of Regina.

‡ National Research Council of Canada.

§ Current address: Istanbul Technical University, Faculty of Science and Literature, Department of Chemistry 34469, Maslak, Istanbul, Turkey.

(1) Frison, G.; Mathey, F.; Sevin, A. *J. Organomet. Chem.* **1998**, *570*, 225.

(2) Ehlers, A. W.; Baerends, E. J.; Lammertsma, K. *J. Am. Chem. Soc.* **2002**, *124*, 2831.

(3) Lammertsma, K.; Vlaar, M. J. M. *Eur. J. Org. Chem.* **2002**, 1127.

(4) Cowley, A. H. *Acc. Chem. Res.* **1997**, *30*, 445.

(5) Hitchcock, P. B.; Lappert, M. F.; Leung, W.-P. *J. Chem. Soc., Chem. Commun.* **1987**, 1282.

(6) (a) Hou, Z.; Stephan, D. W. *J. Am. Chem. Soc.* **1992**, *114*, 10088. (b) Hou, Z.; Breen, T. L.; Stephan, D. W. *Organometallics* **1993**, *12*, 3158. (c) Cummins, C. C.; Schrock, R. R.; Davis, W. M. *Angew. Chem., Int. Ed. Engl.* **1993**, *32*, 756. (d) Breen, T. L.; Stephan, D. W. *J. Am. Chem. Soc.* **1995**, *117*, 11914. (e) Arney, D. S. J.; Schnabel, R. C.; Scott, B. C.; Burns, C. J. *J. Am. Chem. Soc.* **1996**, *118*, 6780. (f) Breen, T. L.; Stephan, D. W. *J. Am. Chem. Soc.* **1996**, *118*, 4204. (g) Urnexius, E.; Lam, K.-C.; Rheingold, A. L.; Protasiewicz, J. D. *J. Organomet. Chem.* **2001**, *630*, 193.

(7) Nakazawa, H.; Buhro, W. E.; Bertrand, G.; Gladysz, J. A. *Inorg. Chem.* **1984**, *23*, 3431.

10.1021/om060685x CCC: $37.00
Publication on Web 01/09/2007

expanded greatly, with new examples of nucleophilic,[14] electrophilic,[15,16] and intermediate[17] phosphinidene complexes being reported. Several new synthetic applications of stable phosphinidene complexes have also been described.[16,18]

As a part of our ongoing studies of the reactivity of terminal phosphinidene complexes, the reactions of $[Cp^*Mo(CO)_3\{PN(i\text{-}Pr)_2\}][AlCl_4]$ (**3**) and $[Cp^*W(CO)_3\{PN(i\text{-}Pr)_2\}][AlCl_4]$ (**4**) with phosphines have been examined. Like Fischer carbenes, the phosphinidene ligands in these complexes have a heteroatom substituent with a lone pair that acts as a π donor to phosphorus. The complexes are expected to be less electrophilic than the transient phosphinidene complexes $[W(CO)_5PR]$ because of the donor properties of the Cp* ring; however, they are still best considered electrophilic phosphinidene complexes on the basis of their structural features: namely, long metal−phosphorus bond lengths and short P−N bond lengths.[13] Our primary goal was to use these reactions and the resulting products as a means of probing the Lewis acid acceptor properties of the aminophosphinidene ligand, but P−P bond forming reactions may also have synthetic utility. Phosphines have been used previously to probe the Lewis acid acceptor ability of low-coordinate phosphorus compounds. For example, phosphine coordination to the phosphorus atom of phosphenium cations has been described[19] and provides a synthetic methodology for P−P bond formation. Phosphine coordination has also been used to form and isolate stable P(I) reagents.[20] The transient electrophilic phosphinidene complexes $[W(CO)_5PR]$ have been trapped with phosphines to form the phosphoranylidenephosphine complexes $[W(CO)_5P(R){=}PR'_3]$.[21] The P−P bond formed in these reactions is clearly a double bond, and the complexes act as "phospha-Wittig" reagents, reacting with organic carbonyl compounds to form phosphaalkenes.[21] The stable rhenium phosphinidene $[Re(CO)_5(PN\{i\text{-}Pr)_2\}]^+$ reacts with triphenylphosphine to form a phosphine adduct with a substantially longer P−P bond of 2.235(1) Å, consistent with a P−P single bond.[16] Donor−acceptor interactions with terminal phosphinidene complexes have also been studied computationally.[11] Portions of this work have been communicated.[22]

Scheme 1

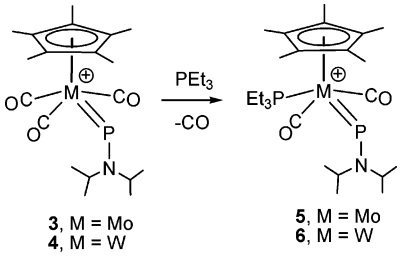

Results and Compound Characterization

The reactions of the molybdenum phosphinidene complex $[Cp^*Mo(CO)_3\{PN(i\text{-}Pr)_2\}][AlCl_4]$ (**3**) and the tungsten phosphinidene complex $[Cp^*W(CO)_3\{PN(i\text{-}Pr)_2\}][AlCl_4]$ (**4**) with triethylphosphine result in carbonyl substitution at the metal to form the phosphine-substituted terminal phosphinidene complexes $[Cp^*Mo(CO)_2(PEt_3)(PN(i\text{-}Pr)_2)][AlCl_4]$ (**5**) and $[Cp^*W(CO)_2(PEt_3)(PN(i\text{-}Pr)_2)][AlCl_4]$ (**6**), in which one metal carbonyl has been replaced by PEt_3 (Scheme 1). Carbonyl loss from the molybdenum complex and formation of **5** is rapid at room temperature. Carbonyl loss from the tungsten complex and formation of **6** require 2 days at room temperature but can be accelerated by heating the solution to 60 °C.

Both compounds have been structurally characterized. An ORTEP diagram of **5** is shown in Figure 1. Crystals of **6** are isomorphous, and its structure is nearly identical with that of **5**. Selected distances and angles for both compounds are given in Table 1. The geometry at the metal is that of a square-based pyramid with two carbonyl groups, the phosphine, and the phosphinidene ligands forming the base and the center of the Cp* ligand occupying the apical position. The phosphine and the phosphinidene ligands are transoid, occupying opposite corners of the square base. The Mo−P and W−P distances to

(8) (a) Kalinina, I.; Donnadieu, B.; Mathey, F. *Organometallics* **2005**, *24*, 696. (b) Compain, C.; Huy, N. H. T.; Mathey, F. *Heteroat. Chem.* **2004**, *15*, 258. (c) Mathey, F. *Angew. Chem., Int. Ed.* **2003**, *42*, 1578. (d) Mathey, F.; Tran Huy, N. H.; Marinetti, A. *Helv. Chim. Acta* **2001**, *84*, 2938. (e) Mathey, F. *Angew. Chem., Int. Ed. Engl.* **1987**, *26*, 275. (f) Borst, M. L. G.; Bulo, R. E.; Winkel, C. W.; Gibney, D. J.; Ehlers, A. W.; Schakel, M.; Lutz, M.; Spek, A. L.; Lammertsma, K. *J. Am. Chem. Soc.* **2005**, *127*, 5800. (g) Borst, M. L. G.; van der Riet, N.; Lemmens, R. H.; de Kanter, F. J. J.; Schakel, M.; Ehlers, A. W.; Mills, A. M.; Lutz, M.; Spek, A. L.; Lammertsma, K. *Chem. Eur. J.* **2005**, *11*, 3631. (h) Borst, M. L. G.; Bulo, R. E.; Gibney, D. J.; Alem, Y.; de Kanter, F. J. J.; Ehlers, A. W.; Schakel, M.; Lutz, M.; Spek, A. L.; Lammertsma, K. *J. Am. Chem. Soc.* **2005**, *127*, 16985. (i) Bulo, R. E.; Ehlers, A. W.; de Kanter, F. J. J.; Schakel, M.; Lutz, M.; Spek, A. L.; Lammertsma, K.; Wang, B. *Chem. Eur. J.* **2004**, *10*, 2732. (j) Bulo, R. E.; Trion, L.; Ehlers, A. W.; de Kanter, F. J. J.; Schakel, M.; Lutz, M.; Spek, A. L.; Lammertsma, K. *Chem. Eur. J.* **2004**, *10*, 5332. (k) Driess, M.; Muresan, N.; Merz, K.; Pach, M. *Angew. Chem., Int. Ed.* **2005**, *44*, 6734.

(9) Marinetti, A.; Mathey, F. *J. Am. Chem. Soc.* **1982**, *104*, 4484.

(10) (a) Ehlers, A. W.; Lammertsma, K.; Baerends, E. J. *Organometallics* **1998**, *17*, 2738. (b) Creve, S.; Pierloot, K.; Nguyen, M. T.; Vanquickenborne, L. G. *Eur. J. Inorg. Chem.* **1999**, 107.

(11) Grigoleit, S.; Alijah, A.; Rozhenko, A. B.; Streubel, R.; Schoeller, W. W. *J. Organomet. Chem.* **2002**, *643*−*644*, 223.

(12) Sterenberg, B. T.; Carty, A. J. *J. Organomet. Chem.* **2001**, *617*−*618*, 696.

(13) Sterenberg, B. T.; Udachin, K. A.; Carty, A. J. *Organometallics* **2001**, *20*, 2657.

(14) (a) Basuli, F.; Tomaszewski, J.; Huffman, J. C.; Mindiola, D. J. *J. Am. Chem. Soc.* **2003**, *125*, 10170. (b) Pikies, J.; Baum, E.; Matern, E.; Chojnacki, J.; Grubba, R.; Robaszkiewicz, A. *Chem. Commun.* **2004**, 2478. (c) Basuli, F.; Bailey, B. C.; Huffman, J. C.; Baik, M. H.; Mindiola, D. J. *J. Am. Chem. Soc.* **2004**, *126*, 1924. (d) Bailey, B. C.; Huffman, J. C.; Mindiola, D. J.; Weng, W.; Ozerov, O. V. *Organometallics* **2005**, *24*, 1390. (e) Wolf, R.; Hey-Hawkins, E. *Eur. J. Inorg. Chem.* **2006**, *2006*, 1348.

(15) (a) Sterenberg, B. T.; Udachin, K. A.; Carty, A. J. *Organometallics* **2003**, *22*, 3927. (b) Sánchez-Nieves, J.; Sterenberg, B. T.; Udachin, K. A.; Carty, A. J. *J. Am. Chem. Soc.* **2003**, *125*, 2404.

(16) Graham, T. W.; Cariou, R. P. Y.; Sanchez-Nieves, J.; Allen, A. E.; Udachin, K. A.; Regragui, R.; Carty, A. J. *Organometallics* **2005**, *24*, 2023.

(17) (a) Melenkivitz, R.; Mindiola, D. J.; Hillhouse, G. L. *J. Am. Chem. Soc.* **2002**, *124*, 3846. (b) Termaten, A. T.; Nijbacker, T.; Schakel, M.; Lutz, M.; Spek, A. L.; Lammertsma, K. *Organometallics* **2002**, *21*, 3196. (c) Termaten, A. T.; Nijbacker, T.; Schakel, M.; Lutz, M.; Spek, A. L.; Lammertsma, K. *Chem. Eur. J.* **2003**, *9*, 2200. (d) Termaten, A. T.; Aktas, H.; Schakel, M.; Ehlers, A. W.; Lutz, M.; Spek, A. L.; Lammertsma, K. *Organometallics* **2003**, *22*, 1827. (e) Termaten, A. T.; Schakel, M.; Ehlers, A. W.; Lutz, M.; Spek, A. L.; Lammertsma, K. *Chem. Eur. J.* **2003**, *9*, 3577. (f) Krautscheid, H.; Matern, E.; Kovacs, I.; Fritz, G.; Pikies, J. *Z. Anorg. Allg. Chem.* **1997**, *623*, 1917. (g) Krautscheid, H.; Matern, E.; Pikies, J.; Fritz, G. *Z. Anorg. Allg. Chem.* **2000**, *626*, 2133. (h) Krautscheid, H.; Matern, E.; Fritz, G.; Pikies, J. *Z. Anorg. Allg. Chem.* **1998**, *624*, 501.

(18) (a) Vlaar, M. J. M.; van Assema, S. G. A.; de Kanter, F. J. J.; Schakel, M.; Spek, A. L.; Lutz, M.; Lammertsma, K. *Chem. Eur. J.* **2002**, *8*, 58. (b) Graham, T. W.; Udachin, K. A.; Carty, A. J. *Chem. Commun.* **2005**, 5890. (c) Menye-Biyogo, R.; Delpech, F.; Castel, A.; Gornitzka, H.; Rivière, P. *Angew. Chem., Int. Ed.* **2003**, *42*, 5610.

(19) (a) David, G.; Niecke, E.; Nieger, M.; Radseck, J. *J. Am. Chem. Soc.* **1994**, *116*, 2191. (b) Burford, N.; Losier, P.; Sereda, S.; Cameron, T. S.; Wu, G. *J. Am. Chem. Soc.* **1994**, *116*, 6474. (c) Burford, N.; Cameron, T. S.; LeBlanc, D. J.; Losier, P.; Sereda, S.; Wu, G. *Organometallics* **1997**, *16*, 4712. (d) Burford, N.; Cameron, T. S.; Ragogna, P. J.; Ocando-Mavarez, E.; Gee, M.; McDonald, R.; Wasylishen, R. E. *J. Am. Chem. Soc.* **2001**, *123*, 7947.

(20) Ellis, B. D.; Carlesimo, M.; Macdonald, C. L. B. *Chem. Commun.* **2003**, 1946.

(21) Le, Floch, P.; Marinetti, A.; Ricard, L.; Mathey, F. *J. Am. Chem. Soc.* **1990**, *112*, 2407.

(22) Sterenberg, B. T.; Udachin, K. A.; Carty, A. J. *Organometallics* **2001**, *20*, 4463.

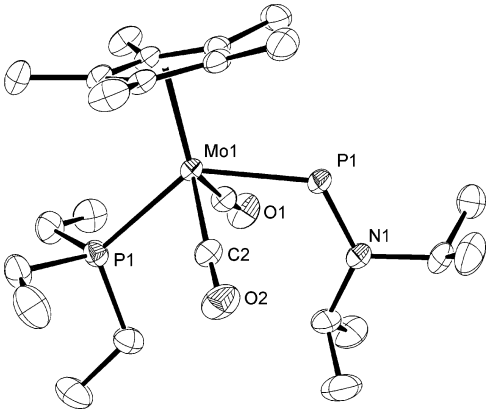

Figure 1. ORTEP diagram of the cation of $[Cp^*Mo(CO)_2(PEt_3)(PN(i\text{-}Pr)_2)][AlCl_4]$ (**5**). Hydrogen atoms have been omitted.

Table 1. Selected Distances (Å) and Angles (deg) in $[Cp^*M(CO)_2(PEt_3)(PN(i\text{-}Pr)_2)][AlCl_4]$

	5 (M = Mo)	**6** (M = W)
M(1)−P(1)	2.3816(4)	2.3846(7)
P(1)−N(1)	1.637(1)	1.634(2)
N(1)−C(3)	1.484(2)	1.490(4)
N(1)−C(6)	1.516(2)	1.518(4)
M(1)−P(2)	2.5086(4)	2.5117(7)
M(1)−C(1)	1.979(1)	1.964(3)
O(1)−C(1)	1.150(2)	1.154(4)
M(1)−C(2)	1.977(1)	1.964(3)
O(2)−C(2)	1.151(2)	1.155(3)
P(1)−M(1)−P(2)	133.16(1)	134.02(2)
C(1)−M(1)-P(1)	74.32(4)	76.10(9)
C(2)−M(1)−P(1)	74.18(4)	73.46(8)
C(2)−M(1)−P(2)	78.52(4)	76.27(8)
C(1)−M(1)−P(2)	78.99(4)	79.8(1)
C(2)−M(1)−C(1)	107.95(6)	105.7(1)
N(1)−P(1)−Mo(1)	121.50(5)	122.06(9)
C(3)−N(1)−C(6)	114.9(1)	114.8(2)
C(3)−N(1)−P(1)	129.2(1)	129.8(2)
C(6)−N(1)−P(1)	115.9(1)	115.3(2)
O(1)−C(1)−M(1)	175.4(1)	176.0(3)
O(2)−C(2)−M(1)	176.2(1)	176.8(2)

the phosphinidene ligand are 2.3816(4) and 2.3846(7) Å, respectively, significantly shorter than the distances observed in the precursor complexes $[Cp^*Mo(CO)_3\{PN(i\text{-}Pr)_2\}][AlCl_4]$ (**3**) (2.4506(4) Å) and $[Cp^*W(CO)_3\{PN(i\text{-}Pr)_2\}][AlCl_4]$ (**4**) (2.4503(6) Å). We will return to the reasons for the shorter bonds in **5** and **6** later in this paper. Other than the metal, the phosphinidene phosphorus atom is bound to nitrogen with P−N bond distances of 1.637(1) and 1.634(2) Å, which are somewhat shorter than typical P−N single bonds[23] but slightly longer than the P−N distances in **3** and **4**. The M−P−NC_2 unit is completely planar within experimental error, and this plane is parallel to the metal−Cp* axis (perpendicular to the Cp* ring). The amine substituent is directed away from the Cp* ring.

The ^{31}P NMR spectrum of **5** shows a broad low-field resonance at δ 957 that corresponds to the terminal phosphinidene ligand. In addition, the metal-bound triethylphosphine ligand results in a resonance at δ 36. The P−P coupling constant is 15 Hz but is only resolved in the sharper PEt_3 resonance. The spectrum of the W analogue **6** is similar, with peaks at δ 878 for the phosphinidene ligand and at δ 6.2 for the triethylphosphine ligand, with a P−P coupling constant of 21 Hz. The PEt_3 resonance at δ 6.2 also exhibits tungsten satellite peaks, with a W−P coupling of 228 Hz. The expected tungsten satellites for the phosphinidene resonance at δ 878 could not be resolved, due to the broadness of the peak. In addition to the expected peaks for the Cp* methyl groups and the ethyl groups of PEt_3, the ^{1}H NMR spectra of the two complexes show two sets of resonances for chemically inequivalent isopropyl groups, consistent with restricted rotation about the P−N bond. This restricted rotation was also observed in the parent compounds **3** and **4** and is attributed to the N−P π-donor interaction.[13]

Scheme 2

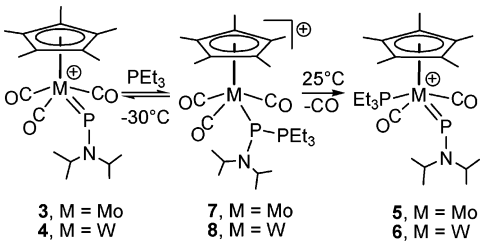

Phosphine substitution at the metal site was contrary to our expectation of nucleophilic attack at the phosphinidene ligand. The reaction of the molybdenum phosphinidene complex with PEt_3 was therefore studied at low temperature. Addition of the phosphine to dark red solutions of **3** at −80 °C resulted in the formation of a yellow solution which upon warming to room temperature evolved gas and changed back to dark red. The ^{31}P NMR spectrum of the yellow product recorded at −30 °C showed two resonances at δ 78.9 and 32.3 with a common coupling constant of 512 Hz. The large coupling constant is indicative of direct P−P bonding and compares with values of 340−455 Hz observed in phosphine-coordinated phosphenium ions[19] and the 361−444 Hz coupling constants observed in phosphoranylidenephosphine complexes formed via the trapping of transient phosphinidene complexes with phosphines.[21] The solution IR spectrum of the yellow intermediate at −30 °C shows three ν(CO) bands at 2013, 1947, and 1917 cm^{-1}, indicating that the three carbonyls of the starting material are retained. The initial site of attack by the phosphine is therefore at the phosphinidene phosphorus, as expected, forming $[Cp^*Mo(CO)_3\{P(PEt_3)N(i\text{-}Pr)_2\}][AlCl_4]$ (**7**) (Scheme 2). When the temperature is raised, a carbonyl is lost and the phosphine ligand migrates from the phosphinidene ligand to the metal. The coordination of the phosphine to the phosphinidene is thus reversible.

In the tungsten complex, carbonyl loss to form the final product is much slower, suggesting that the intermediate complex $[Cp^*W(CO)_3\{P(PEt_3)N(i\text{-}Pr)_2\}][AlCl_4]$ (**8**) has a longer lifetime and therefore might be observed at room temperature. However, at room temperature only a single very broad peak at δ −15 is observed in the ^{31}P NMR spectrum, because coordination of the phosphine to the phosphinidene is rapidly reversible and the phosphine-coordinated phosphinidene **8** is in rapid equilibrium with the free phosphinidene complex **4** and triethylphosphine (see Scheme 2). The observed peak is the average of resonances for free triethylphosphine and triethylphosphine coordinated to the phosphinidene. A resonance for the phosphinidene phosphorus is not observed and is presumed to be very broad at room temperature, as a result of the very large chemical shift difference. At low temperature, **8** is readily observed and shows spectroscopic parameters similar to those of the molybdenum intermediate **7**. Irreversible carbonyl loss from **8** then leads to the final product **6**.

Although the triethylphosphine-coordinated phosphinidene complexes have been spectroscopically characterized, crystal-

(23) Orpen, A. G.; Brammer, L.; Allen, F. H.; Kennard, O.; Watson, D. G.; Taylor, R. *J. Chem. Soc., Dalton Trans.* **1989**, S1.

Scheme 3

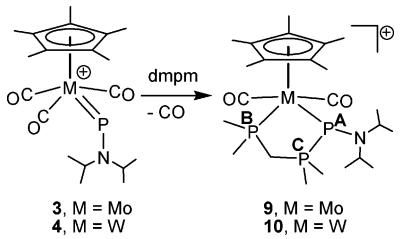

lographically characterized examples were also of interest to us. Compounds **3** and **4** were thus reacted with the diphosphine bis(dimethylphosphino)methane (dmpm), leading to the complexes $[Cp^*Mo(CO)_2\{P(N(i\text{-}Pr)_2)P(Me_2)CH_2P(Me_2)\text{-}\kappa^2P^1,P^4\}][AlCl_4]$ (**9**) and $[Cp^*W(CO)_2\{P(N(i\text{-}Pr)_2)P(Me_2)CH_2P(Me_2)\text{-}\kappa^2P^1,P^4\}][AlCl_4]$ (**10**), in which the two ends of the dmpm ligand coordinate to the phosphinidene phosphorus and the metal, respectively (Scheme 3). The ^{31}P NMR spectrum of **9** (Figure 2) shows three resonances at δ 109.3 (P^A), 41.2 (P^B), and 10.8 (P^C). A very large one-bond coupling of 532 Hz is observed between P^A and P^C, while P^C and P^B share a two-bond P−P coupling of 98 Hz across the dmpm methylene group. Finally, a two-bond coupling of 13 Hz is observed between the two metal-bound phosphorus atoms. The ^{31}P NMR spectrum of the tungsten complex **10** is similar but additionally shows tungsten−phosphorus coupling constants of 136, 249, and 27 Hz, respectively, for P^A, P^B, and P^C. The ^1H NMR spectra of both compounds show two chemically equivalent isopropyl groups, as indicated by a single CH resonance, suggesting that there is free rotation about the P−N bond. Although P^A is chiral, the ^1H NMR spectra shows no evidence for diastereotopic isopropyl groups because of facile inversion at N. The dmpm methylene hydrogens and the dmpm methyl groups are chemically inequivalent as a result of the lack of symmetry in the complex, regardless of chirality at P^A.

Characterization of the compound **9·[AlCl$_4$]** by X-ray crystallography was attempted, but twinning problems could not be satisfactorily resolved. Exchange of the $AlCl_4^-$ counterion for BPh_4^- allowed high-quality single crystals of $[Cp^*Mo(CO)_2\{P(N(i\text{-}Pr)_2)P(Me_2)CH_2P(Me_2)\text{-}\kappa^2P^1,P^4\}][BPh_4]$ (**9·[BPh$_4$]**) to be grown. An ORTEP diagram of the cation is shown in Figure 3, and selected distances and angles are shown in Table 2. The geometry at the metal is again that of a square-based pyramid, with the phosphine and the phosphine-coordinated phosphinidene ligands in a cisoid arrangement. The molybdenum, the three phosphorus atoms, and the methylene carbon form a puckered five-membered ring. The Mo(1)−P(1) distance of 2.5430(7) Å has lengthened considerably compared to the Mo−P distance of 2.4506(4) Å in the phosphinidene complex **3**, consistent with an Mo−P single bond. This distance is in fact longer than the Mo−phosphine distance in the same complex (Mo(1)−P(3) = 2.4585(6) Å).

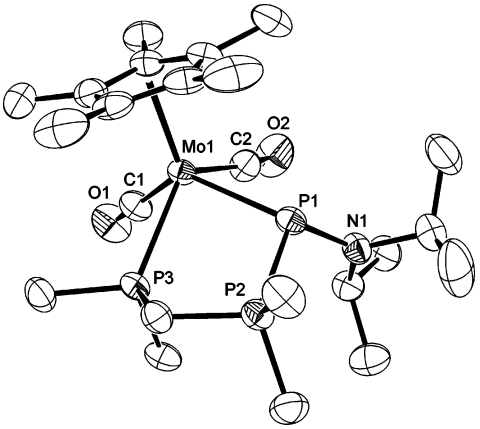

Figure 3. ORTEP diagram of the cation of $[Cp^*Mo(CO)_2\{P(N(i\text{-}Pr)_2)P(Me_2)CH_2P(Me_2)\text{-}\kappa^2P^1,P^4\}][BPh_4]$ (**9**). Hydrogen atoms have been omitted.

Table 2. Selected Distances (Å) and Angles (deg) in $[Cp^*M(CO)_2\{P(N(i\text{-}Pr)_2)P(Me_2)CH_2P(Me_2)\text{-}\kappa^2P^1,P^4\}][X]$

	9 (M = Mo, X = BPh)	**10** (M = W, X = $AlCl_4$)
M(1)−P(1)	2.5430(7)	2.5448(6)
M(1)−P(3)	2.4585(6)	2.4441(6)
M(1)−C(1)	1.951(3)	1.945(3)
M(1)−C(2)	1.957(3)	1.963(3)
P(1)−N(1)	1.684(2)	1.681(2)
P(1)−P(2)	2.2664(8)	2.2236(9)
O(1)−C(1)	1.159(3)	1.164(3)
O(2)−C(2)	1.147(3)	1.158(3)
C(1)−M(1)−C(2)	74.9(1)	76.1(1)
C(1)−M(1)−P(3)	74.96(7)	75.61(8)
C(2)−M(1)−P(3)	120.89(8)	121.22(8)
C(1)−M(1)−P(1)	129.55(8)	130.03(8)
C(2)−M(1)−P(1)	81.02(8)	80.81(8)
P(3)−M(1)−P(1)	80.78(2)	79.83(2)
N(1)−P(1)−P(2)	108.03(8)	107.2(1)
N(1)−P(1)−Mo(1)	121.30(8)	125.04(9)
P(2)−P(1)−Mo(1)	107.68(3)	109.81(3)
C(6)−N(1)−C(3)	116.1(2)	115.4(2)
C(6)−N(1)−P(1)	126.2(2)	126.5(2)
C(3)−N(1)−P(1)	117.6(2)	117.9(2)
O(1)−C(1)−M(1)	177.8(2)	177.9(2)
O(2)−C(2)−M(1)	170.4(2)	171.7(2)

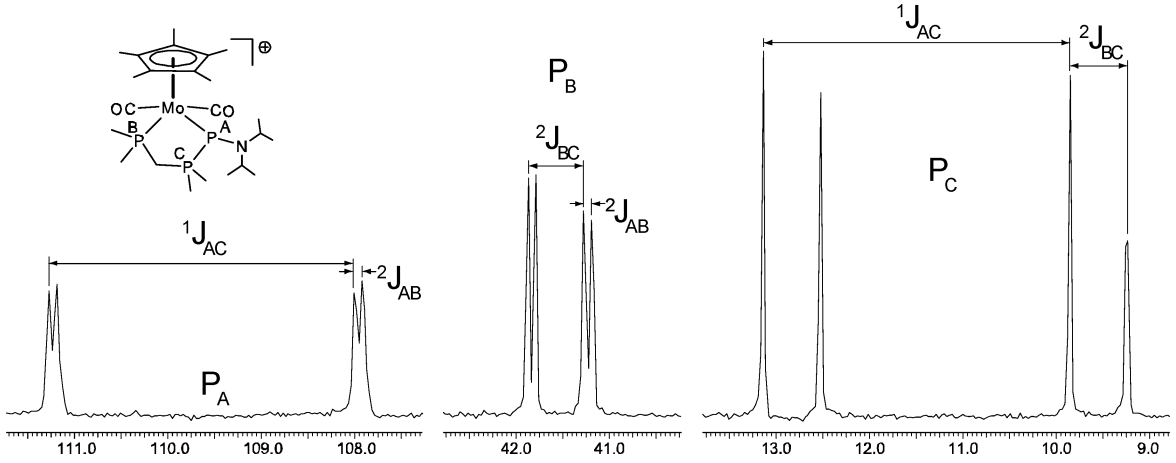

Figure 2. $^{31}P\{^1H\}$ NMR spectrum of $[Cp^*Mo(CO)_2\{P(N(i\text{-}Pr)_2)P(Me_2)CH_2P(Me_2)\text{-}\kappa^2P^1,P^4\}][AlCl_4]$ (**9**).

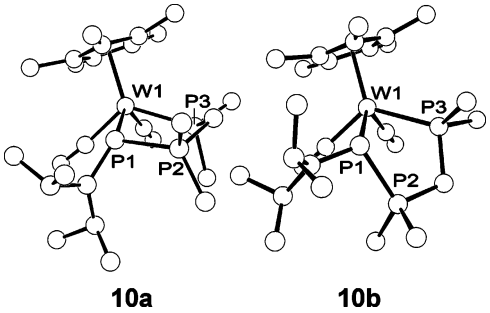

Figure 4. Isomers of [Cp*W(CO)$_2${P(N(*i*-Pr)$_2$)P(Me$_2$)CH$_2$P(Me$_2$)-κ^2P^1,P^4}][AlCl$_4$] (**10**).

Scheme 4

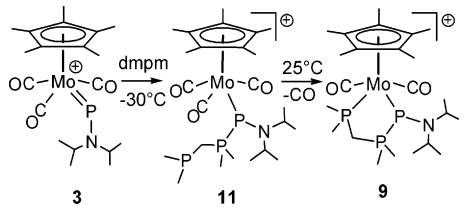

The P(1)−P(2) distance of 2.2664(8) Å is within the typical range observed for P−P single bonds (for example, P−P bonds in diphosphines fall in the range 2.205(1)−2.260(1) Å[23]). The P−P distance in **9** is significantly longer than the P−P distance of 2.156(2) Å observed in Et$_3$P═P(CO$_2$Et)W(CO)$_5$, which was formed by trapping the transient phosphinidene W(CO)$_5$(PCO$_2$-Et) with PEt$_3$.[21] In addition to P(2) and Mo, P(1) is bound to the diisopropyl amino group with a P−N bond distance of 1.684(2) Å, which is longer than the P−N distance of 1.631(1) Å in the starting phosphinidene complex **1** and is now consistent with a P−N single bond.[23] The geometry at P(1) is pyramidal, clearly indicating the presence of a stereoactive lone pair.

High-quality crystals of the tungsten analogue **10** were grown with the AlCl$_4^-$ counterion. In the solid state, compound **10** exists as two isomers, which were separated by selecting single crystals from the mixture. The isomers differ in the conformation of the five-membered ring formed by the metal, the dmpm, and the phosphinidene phosphorus atom (see Figure 4). Isomer **10a** shows the same conformation as **9**. Isomer **10b** differs from **10a** by a 120° rotation about the metal−phosphine bond, resulting in the methylene bridge being oriented away from the Cp* ring and the diisopropylamino group on the phosphinidene phosphorus being directed toward the Cp* ring. Both isomers have been structurally characterized, but the data for **10b** were of poorer quality. Reported distances therefore refer to isomer **10a**. Variable-temperature NMR spectroscopy shows no evidence of multiple isomers of **10** in solution, suggesting that this isomerization occurs upon crystallization of **10**. A second isomer of the Mo analogue **9** was not observed; however, we cannot rule out the possibility that it does form in the solid state.

As with the triethylphosphine reaction described above, the reaction of [Cp*Mo(CO)$_3${PN(*i*-Pr)$_2$}][AlCl$_4$] (**3**) with dmpm was examined at low temperature. The initial site of attack is again at the phosphinidene phosphorus, and the phosphine adduct [Cp*Mo(CO)$_3${P(N(*i*-Pr)$_2$)P(Me$_2$)CH$_2$P(Me$_2$)-κP^1}][AlCl$_4$] (**11**) was observed at low temperature as the initial product in the reaction (Scheme 4). The ^{31}P NMR spectrum of **11** shows three resonances. The phosphinidene resonance appears at δ 97.2 and with a large P−P coupling constant of 506 Hz, indicative of a direct P−P bond. The end of the diphosphine that coordinates to the phosphinidene phosphorus atom appears at δ 17.1 as a doublet of doublets with the 506 Hz coupling to the phosphinidene phosphorus atom, as well as a 34 Hz P−P coupling across the methylene group to the P atom at the other end of the dmpm ligand. The phosphorus resonance for the dangling end of dmpm appears at δ −49.6, close to the chemical shift of free dmpm. The IR spectrum of **11** contains three carbonyl stretching bands at 2004, 1935, and 1919 cm^{-1}, very similar to those of compound **7**. When the compound is warmed to room temperature, evolution of gas is observed and the color changes from yellow to orange with the formation of **9**.

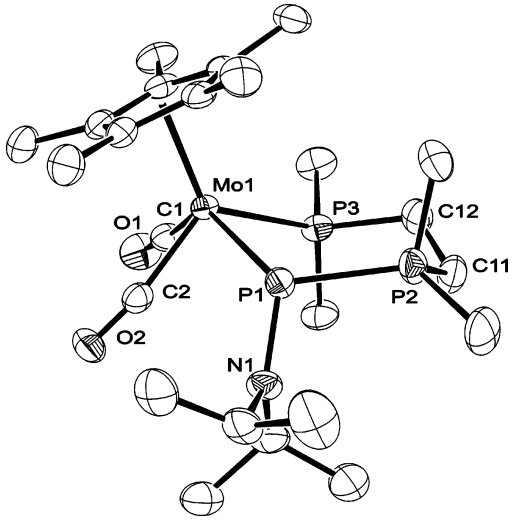

Figure 5. ORTEP diagram of the cation of [Cp*Mo(CO)$_2${P(N(*i*-Pr)$_2$)P(Me$_2$)CH$_2$CH$_2$P(Me$_2$)-κ^2P^1,P^5}][AlCl$_4$] (**12**). Hydrogen atoms have been omitted.

The analogous reactions of the terminal phosphinidene complexes were also carried out with bis(dimethylphosphino)-ethane (dmpe), which differs from dmpm in having an additional methylene group in its backbone. While dmpm has a strong tendency to bridge, the larger bite angle of dmpe favors chelation, opening the possibility of different coordination modes for the diphosphine. The molybdenum phosphinidene complex [Cp*Mo(CO)$_3${PN(*i*-Pr)$_2$}][AlCl$_4$] (**3**) reacts cleanly with dmpe to form [Cp*Mo(CO)$_2${P(N(*i*-Pr)$_2$)P(Me$_2$)CH$_2$CH$_2$P-(Me$_2$)-κ^2P^1,P^5}][AlCl$_4$] (**12**), which is analogous to **9**, with the diphosphine ligand bridging between the phosphinidene phosphorus and the metal. The ORTEP diagram of the cation is shown in Figure 5, and selected distances and angles are given in Table 3. The geometry at the metal is again that of a square-based pyramid, with the phosphine and the coordinated phosphinidene in a cisoid arrangement. The molybdenum, the three phosphorus atoms, and two methylene carbons form a six-membered ring with a roughly chair-shaped conformation. The P(1)−P(2) distance of 2.2149(9) Å is slightly shorter than that observed for **9** (2.2664(8) Å) but is still consistent with a single bond. The Mo−P(1) distance of 2.5835(6) Å is slightly longer than that in **9** (2.5430(7) Å). These bond length differences are likely due to steric factors resulting from the different ring sizes and are not chemically significant. The P(1)−N(1) distance of 1.688(2) Å is very close to that observed for **9**.

The ^{31}P NMR spectrum of **12** shows broad resonances for three unique phosphorus atoms at δ 56.8, 2.3, and −2.7. The high- and low-field peaks have a common coupling constant of 614 Hz, indicative of a one-bond P−P coupling and a direct P−P bond. In addition, a three-bond coupling of 39 Hz is observed between the two highest field peaks, which is due to coupling across the CH$_2$CH$_2$ backbone of the dmpe ligand. The coupling constants allow assignment of the peak at δ 56.8 as the phosphinidene phosphorus, that at δ −2.7 as the phosphine

Table 3. Selected Distances (Å) and Angles (deg) in [Cp*M(CO)$_2${P(N(*i*-Pr)$_2$)P(Me$_2$)CH$_2$CH$_2$P(Me$_2$)-κ^2P^1,P^5}][AlCl$_4$]

	12 (M = Mo)	**13** (M = W)
Mo−P(1)	2.5835(6)	2.573(2)
Mo−P(3)	2.5167(7)	2.509(2)
Mo−C(2)	1.953(3)	1.958(7)
Mo−C(1)	1.956(3)	1.966(7)
P(1)−N	1.688(2)	1.687(6)
P(1)−P(2)	2.2149(9)	2.216(3)
O(1)−C(1)	1.157(3)	1.147(9)
O(2)−C(2)	1.152(3)	1.154(9)
C(2)−Mo−C(1)	74.95(11)	74.8(3)
C(2)−Mo−P(3)	74.00(9)	73.5(2)
C(1)−Mo−P(3)	117.24(8)	117.6(2)
C(2)−Mo−P(1)	133.98(8)	133.4(2)
C(1)−Mo−P(1)	76.32(7)	76.6(2)
P(3)−M−P(1)	88.47(2)	88.45(6)
N−P(1)−P(2)	106.09(9)	106.0(2)
N−P(1)−Mo	118.41(8)	118.2(2)
P(2)−P(1)−Mo	111.21(3)	111.66(9)

Scheme 5

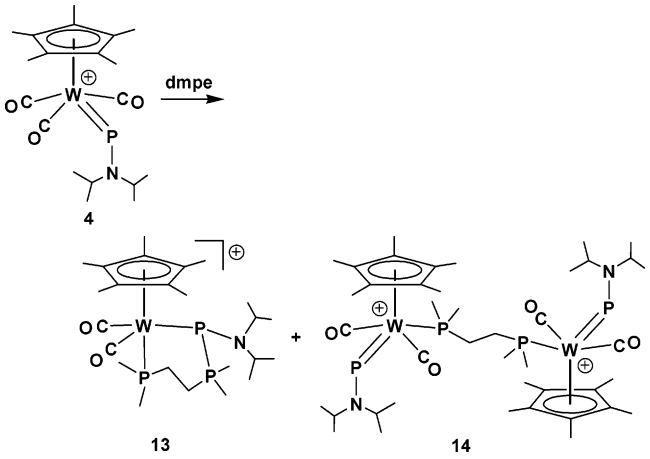

coordinated to it, and the third peak at δ 2.3 as the metal-coordinated phosphine. The two-bond coupling constant between the metal-bound P atoms is masked by the broadness of the peaks.

Because of the broadness of the peaks at room temperature, the spectrum was examined at low temperature. At −90 °C, each resonance is resolved into two, suggesting the presence of two rapidly interconverting isomers. The spectrum is still broad at −90 °C, indicating that the low-temperature limiting spectrum has not been reached and that the interconversion process is very facile. One isomer, **12a**, shows three peaks at δ 50.8, 2.9, and 2.1 with P−P coupling constants of 617 and 15 Hz. The second isomer, **12b**, shows three peaks at δ 44.8, −1.2, and −6.8 with couplings of 623 and 77 Hz. Clearly, the two isomers have similar structures and the isomerization process does not involve dissociation of the P−P bond, since the coupling constant is maintained in the high-temperature spectrum. Metal−phosphine dissociation cannot be entirely ruled out, since no coupling is observed between the metal-bound phosphorus atoms; however, it is unlikely to be so facile. The significant difference between the coupling constants across the dmpe ligand in the two isomers suggests that the isomerization simply involves rearrangement of the CH_2CH_2 linkage, as shown in Figure 6: effectively chair versus boat rearrangement of the six-membered ring. The solid-state structure, which shows the chair configuration, can be assigned to isomer **12b** on the basis of the larger P−P coupling across the dmpe backbone (77 Hz), which results from a "w" coupling.[24] The boat conformation of

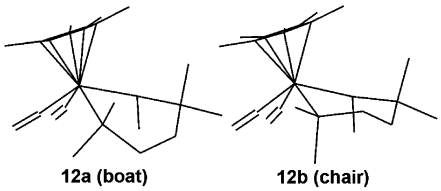

Figure 6. Optimized boat and chair conformations of [Cp*Mo(CO)$_2${P(N(*i*-Pr)$_2$)P(Me$_2$)CH$_2$CH$_2$P(Me$_2$)-κ^2P^1,P^5}][AlCl$_4$] (**12**). Hydrogen atoms and isopropyl groups have been omitted for clarity.

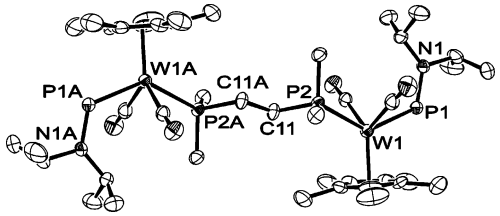

Figure 7. ORTEP diagram of the cation of [{Cp*W(CO)$_2$(PN(*i*-Pr)$_2$)}$_2$(μ-dmpe)][AlCl$_4$]$_2$ (**14**). Hydrogen atoms have been omitted.

Table 4. Selected Distances (Å) and Angles (deg) in [{Cp*W(CO)$_2$(PN(*i*-Pr)$_2$)}$_2$(μ-dmpe)][AlCl$_4$]$_2$ (14)

W(1)−P(1)	2.386(1)	P(2)−C(10)	1.818(4)
W(1)−P(2)	2.498(1)	P(2)−C(11)	1.834(4)
W(1)−C(1)	1.991(4)	O(1)−C(1)	1.138(5)
W(1)−C(2)	1.985(5)	O(2)−C(2)	1.138(6)
P(1)−N(1)	1.635(4)	C(11)−C(11A)	1.546(8)
P(2)−C(9)	1.810(4)		
C(2)−W(1)−C(1)	109.4(2)	P(1)−W(1)−P(2)	133.13(4)
C(2)−W(1)−P(1)	75.2(1)	N(1)−P(1)−W(1)	121.6(1)
C(1)−W(1)−P(1)	78.2(1)	C(3)−N(1)−C(6)	115.4(3)
C(17)−W(1)−P(1)	85.3(1)	C(3)−N(1)−P(1)	129.3(3)
C(18)−W(1)−P(1)	119.9(1)	C(6)−N(1)−P(1)	115.2(3)
C(16)−W(1)−P(1)	79.7(1)	O(1)−C(1)−W(1)	175.6(4)
C(2)−W(1)−P(2)	75.5(1)	O(2)−C(2)−W(1)	176.2(4)
C(1)−W(1)−P(2)	78.1(1)		

isomer **12a** exhibits a smaller P−P coupling of 15 Hz. The more rigid five-membered ring of the analogous dmpm complex **9** does not show any isomerization.

Reaction of the tungsten phosphinidene complex with dmpe led to a mixture of products (Scheme 5). The major product, [Cp*W(CO)$_2${P(N(*i*-Pr)$_2$)P(Me$_2$)CH$_2$CH$_2$P(Me$_2$)-κ^2P^1,P^5}][AlCl$_4$] (**13**) is analogous to the product of the Mo reaction, containing a dmpe ligand that bridges the metal and the phosphinidene phosphorus. Compound **13** has been completely characterized, including the X-ray crystal structure (see Table 3 for selected distances and angles and the Experimental Section for spectroscopy).

A second product was isolated and was shown to be the binuclear complex [{Cp*W(CO)$_2$(PN(*i*-Pr)$_2$)}$_2$(μ-dmpe)][AlCl$_4$]$_2$ (**14**), which consists of two tungsten terminal phosphinidene complexes bridged by a dmpe ligand that has substituted a carbonyl ligand on each of the metals. Compound **14** has been structurally characterized, and an ORTEP diagram of the cation is shown in Figure 7. Selected distances and angles are given in Table 4. The molecule lies on a crystallographic center of symmetry, and both tungsten centers are crystallographically equivalent. The geometry at tungsten is very similar to that in the triethylphosphine complexes **5** and **6**, with the two phosphorus ligands occupying opposite corners of the four-legged piano stool. The tungsten−phosphinidene distance of 2.386(1) Å is nearly identical with that in **6** (2.3846(7) Å) and

(24) Jameson, C. J. In *Phosphorus-31 NMR Spectroscopy in Stereochemical Analysis*; Verkade, J. G., Quin, L. D., Eds.; VCH: Deerfield Beach, FL, 1987.

Scheme 6

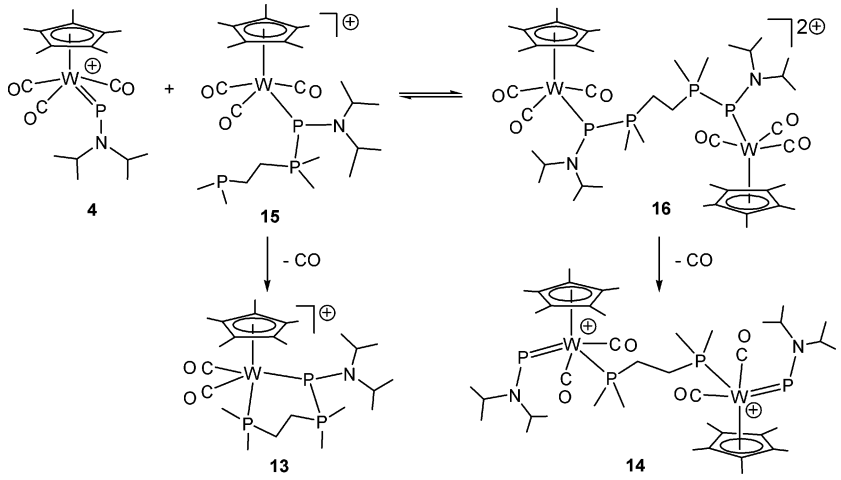

Scheme 7

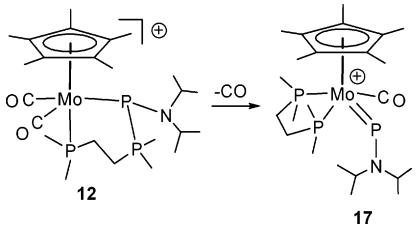

substantially shorter than the W−P distance in the starting phosphinidene complex **4** (2.4503 Å). The P−N distance of 1.635(4) Å is slightly longer than that of the unsubstituted phosphinidene complex (1.629(2) Å). This complex shows ^{31}P NMR parameters similar to those of the triethylphosphine-substituted complex **6** with doublets at δ 890 and −7, corresponding to the phosphinidene phosphorus and the phosphine, respectively. The coupling constant of 10 Hz and the low-field shift of the phosphinidene phosphorus clearly indicate that the phosphine is coordinated to the metal and not to the phosphinidene phosphorus.

We suggest that **14** arises from initial coordination of the phosphine to the phosphinidene phosphorus, followed by coordination of the other end of the phosphine to a second equivalent of the phosphinidene complex (Scheme 6). This second coordination occurs in the tungsten complexes and not the molybdenum complexes, because carbonyl loss to form the chelate is much slower for tungsten. Since both ends of the phosphine are coordinated in the intermediate, carbonyl loss from the metal leads to migration of the phosphine from the phosphinidene to the metal, rather than chelate formation. The intermediate **16** can be readily detected at low temperature by reaction of [Cp*W(CO)$_3${PN(*i*-Pr)$_2$}][AlCl$_4$] (**4**) with less than 0.5 equiv of dmpe at −80 °C. The ^{31}P NMR spectrum of **16** shows two resonances at δ 58 and 17.9, with a common coupling constant of 523 Hz, resulting from the direct P−P bond. At −80 °C, **16** is in rapid equilibrium with [Cp*W(CO)$_3${PN(*i*-Pr)$_2$}][AlCl$_4$] (**4**) and [Cp*W(CO)$_2${P(N(*i*-Pr)$_2$)P(Me$_2$)CH$_2$-CH$_2$P(Me$_2$)-κP^1}][AlCl$_4$] (**15**) (see Scheme 6). At temperatures above −80 °C, the left-hand side of this equilibrium is favored, meaning that warming solutions of **16** to room temperature does not lead primarily to **14** but to **13**. Compound **14** can be isolated in 20% yield if [Cp*W(CO)$_3${PN(*i*-Pr)$_2$}][AlCl$_4$] (**4**) is reacted with less than 0.5 equiv of dmpe at very high concentration. Reaction of the molybdenum analogue [Cp*Mo(CO)$_3${PN(*i*-Pr)$_2$}][AlCl$_4$] (**3**) with dmpe under the same experimental conditions does not lead to a Mo analogue of **14** but simply leads to a mixture of **12** and **3**.

Table 5. Selected Distances (Å) and Angles (deg) in [Cp*Mo(CO)(PN(*i*-Pr)$_2$)(dmpe-κ^2P)][AlCl$_4$] (17)

Mo(1)−P(1)	2.3568(4)	O(1)−C(1)	1.167(2)
Mo(1)−P(2)	2.4871(4)	P(2)−C(10)	1.858(2)
Mo(1)−P(3)	2.4856(4)	P(3)−C(11)	1.829(2)
Mo(1)−C(1)	1.939(2)	C(10)−C(11)	1.526(3)
P(1)−N(1)	1.651(1)		
C(1)−Mo(1)−P(1)	74.98(5)	C(10)−P(2)−Mo(1)	111.60(6)
C(1)−Mo(1)−C(15)	124.80(6)	C(11)−P(3)−Mo(1)	108.26(6)
C(1)−Mo(1)−P(3)	75.84(5)	C(5)−N(1)−C(2)	114.4(1)
P(1)−Mo(1)−P(3)	128.70(1)	C(5)−N(1)−P(1)	128.9(1)
C(1)−Mo(1)−P(2)	116.81(5)	C(2)−N(1)−P(1)	116.7(1)
P(1)−Mo(1)−P(2)	83.15(1)	O(1)−C(1)−Mo(1)	172.3(1)
P(3)−Mo(1)−P(2)	73.77(1)	C(11)−C(10)−P(2)	112.8(1)
N(1)−P(1)−Mo(1)	125.09(5)	C(10)−C(11)−P(3)	112.0(1)

Although the molybdenum dmpm complex **9** is stable, the dmpe complex **12** shows a tendency to decompose. One decomposition product was isolated that results from CO loss and migration of the other end of the dmpe ligand to the metal, regenerating a free phosphinidene ligand (see Scheme 7). The reaction can also be induced by photolysis.

The complex [Cp*Mo(CO)(PN(*i*-Pr)$_2$)(dmpe-κ^2P)][AlCl$_4$] (**17**) has been structurally characterized, and an ORTEP diagram of the cation is shown in Figure 8. Selected distances and angles are given in Table 5. The compound is analogous to the starting phosphinidene [Cp*Mo(CO)$_3${PN(*i*-Pr)$_2$}][AlCl$_4$] (**3**), except that

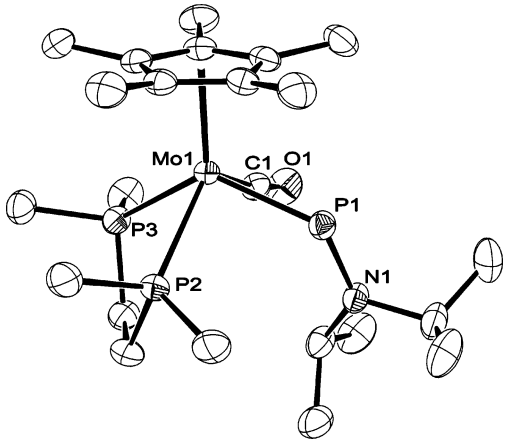

Figure 8. ORTEP diagram of the cation of [Cp*Mo(CO)(PN(*i*−Pr)$_2$)(dmpe-κ^2P)][AlCl$_4$] (**17**). Hydrogen atoms have been omitted.

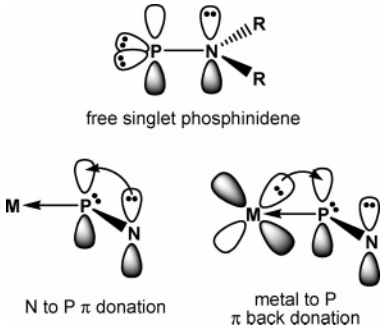

Figure 9. Bonding in free triplet phosphinidene and electrophilic phosphinidene complexes.

two carbonyls have been replaced by two ends of the chelating dmpe ligand. The geometry at the metal is again that of a four-legged piano stool. The dmpe ligand occupies two adjacent legs, while the phosphinidene and carbonyl ligands occupy the other two. The Mo−P distance to the phosphinidene ligand is 2.3568(4) Å, significantly shorter than that in **3** (2.4506(4) Å). The P−N distance in the phosphinidene ligand of 1.651(1) Å is longer than that in complex **3** (1.631(1) Å). In contrast to those in **3**−**6** and **14**, the aminophosphinidene ligand in **17** deviates slightly from planarity in that the N(*i*-Pr)$_2$ unit has rotated about the P−N bond by 4.0(1)°. The entire phosphinidene unit has also rotated about the Mo−P bond relative to the metal−Cp* axis by 15.61(6)°, such that the P−N vector does not point directly away from the Cp* ring as it does in all of the other terminal phosphinidene complexes. These deviations are likely a result of steric interactions with the methyl groups on the adjacent end of the dmpe ligand. In the other complexes, the terminal phosphinidene ligand is adjacent only to carbonyls.

The resonance for the phosphinidene ligand in **17** appears at δ 1058 in the ^{31}P NMR spectrum, the highest ^{31}P chemical shift of any of the complexes reported here. The two ends of the dmpe ligand are chemically inequivalent and couple to each other with a coupling constant of 37 Hz. Each also shows a small P−P coupling (11 and 13 Hz, respectively) to the phosphinidene phosphorus. These small couplings are masked by the broadness of the phosphinidene peak. The infrared spectrum shows a peak at 1883 cm^{-1} for the single carbonyl ligand. In the ^{1}H NMR, the two isopropyl groups of the aminophosphinidene ligand are chemically inequivalent, as was observed for all the other terminal aminophosphinidene complexes.

Discussion

In all cases, the reaction of the terminal phosphinidene complexes with a phosphine results in initial attack by the phosphine nucleophile at the phosphinidene phosphorus atom. This reactivity is consistent with the formulation of the terminal phosphinidenes as electrophilic phosphinidenes. Computational studies[1] have shown that the LUMO of a terminal electrophilic phosphinidene complex is primarily phosphorus-based, consistent with nucleophilic attack at phosphorus, as is observed experimentally in our systems. The bonding in electrophilic phosphinidenes is best conceptualized by considering the ligands to be derived from the singlet state of free phosphinidene, which contains two lone pairs and an empty p_z orbital. One lone pair forms a σ-donor interaction to the transition metal while the second lone pair remains stereoactive, leading to the bent geometry at phosphorus. The empty p_z orbital is then capable of accepting π-donation from a heteroatom substituent or from filled metal d orbitals (Figure 9).

Table 6. Structural and Spectroscopic Parameters for Phosphine-Coordinated Phosphinidene Complexes[a]

compd	*d*(M−P)	*d*(P−N)	*d*(P−P)	δ(^{31}P)	$^1J_{PP}$ (Hz)
3	2.4506(4)	1.631(1)		1007.5	
4	2.4503(6)	1.629(2)		939.4	
9	2.5430(7)	1.684(2)	2.2664(8)	109.3	532
10	2.5448(6)	1.681(2)	2.2236(9)	91.4	570
12	2.5835(6)	1.688(2)	2.2149(9)	56.8	614
13	2.573(2)	1.687(6)	2.216(3)	34.7	607

[a] For comparison, the base-free phosphinidene complexes **3** and **4** are included.

Coordination of a phosphine to the phosphinidene results in occupation of the empty phosphinidene p orbital and has profound effects on the structural and spectroscopic parameters of the phosphinidene ligand. These changes are summarized in Table 6, for stable chelated phosphine-coordinated phosphinidene complexes. Structurally, phosphine coordination at the phosphinidene results in a substantial lengthening of the metal−phosphorus bond from 2.45 Å in the base-free phosphinidene complexes to 2.54−2.58 Å in the phosphine-coordinated complexes. This indicates that the base-free phosphinidene ligand has significant π-acceptor capabilities and accepts π-back-donation from the metal. Phosphine coordination to the phosphinidene eliminates the possibility of π-back-donation by occupying the empty phosphorus p_z orbital, resulting in a lengthening of the bond. The occupation of this empty orbital also eliminates the possibility of nitrogen to phosphorus π-donation. This change is reflected in an increase of the P−N distance of approximately 0.05 Å. Spectroscopically, phosphine coordination results in a large change in the chemical shift to lower frequency by about 850−950 ppm.

Phosphine coordination to the phosphinidene phosphorus also results in labilization of a metal-bound carbonyl, as indicated by the ready loss of a carbonyl ligand below room temperature from the intermediate [Cp*Mo(CO)$_3${P(PEt$_3$)N(*i*-Pr)$_2$}][AlCl$_4$] (**7**). Carbonyl loss from the analogous tungsten intermediate **8** is slower but still favorable. A comparison of the ν(CO) frequencies of the PEt$_3$-coordinated intermediate [Cp*Mo(CO)$_3$-{P(PEt$_3$)N(*i*-Pr)$_2$}][AlCl$_4$] (**7**) (2013, 1947, and 1917 cm^{-1}) with those of the starting phosphinidene complex [Cp*Mo(CO)$_3${PN-(*i*-Pr)$_2$}][AlCl$_4$] (**3**) (2041, 1986, and 1959 cm^{-1}) shows a significant shift to lower frequency upon coordination of the phosphine to the phosphinidene. This shift to lower frequency is consistent with a reduction in the π-back-bonding to the phosphinidene from the metal as the empty phosphorus p orbital is occupied by the incoming electron pair and subsequently results in an increase in π-back-bonding to the carbonyl ligands from the metal. However, it does not explain the lability of the carbonyl ligand in **7**, as the increased π-back-bonding to the carbonyls would be expected to increase the metal−carbon bond strength. The lability of the carbonyl in **7** is attributed rather to a stabilization of the 16-electron intermediate **B**, formed upon carbonyl loss by the lone pair of the phosphine-coordinated phosphinidene ligand (Scheme 8). The lone pair of the base-free phosphinidene ligand, given its electrophilic nature, is too low in energy to provide the same stabilization to intermediate **A** and facilitate carbonyl loss from **3**. This proposed mechanism has been supported with computational studies. Energies were calculated for [Cp*Mo(CO)$_3${PN(*i*-Pr)$_2$}]$^+$ (**3**) and [Cp*Mo-(CO)$_3${P(PEt$_3$)N(*i*-Pr)$_2$}]$^+$ (**7**) and for the proposed intermediates that result from carbonyl loss from **3** and **7,** [Cp*Mo(CO)$_2$-{PN(*i*-Pr)$_2$}]$^+$ (**A**) and [Cp*Mo(CO)$_2${P(PEt$_3$)N(*i*-Pr)$_2$}]$^+$ (**B**). The energy for carbonyl loss from the phosphine-coordinated phosphinidene is lower by 3.5 kJ/mol than the energy of carbonyl loss from the base-free phosphinidene. The optimized

Scheme 8

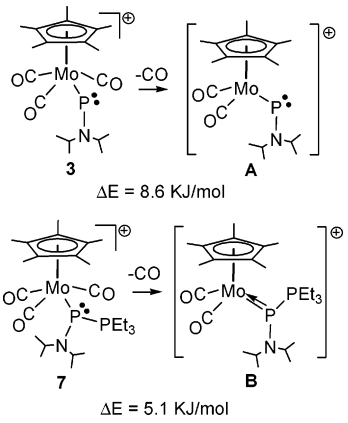

Table 7. Structural Parameters for Phosphinidene Complexes $[Cp^*M\{PN(i\text{-}Pr)_2\}(CO)_mL_n]^+$

compd	*d*(M−P)	*d*(P−N)	M	m	n
3	2.4506(4)	1.631(1)	Mo	3	0
5	2.3816(4)	1.637(1)	Mo	2	1
17	2.3568(4)	1.651(1)	Mo	1	2
4	2.4503(6)	1.629(2)	W	3	0
6	2.3846(7)	1.634(2)	W	2	1
14	2.386(1)	1.635(4)	W	2	1

structure of intermediate **B** also shows a short Mo−P bond of 2.32 Å, consistent with an Mo−P double bond, and a planar geometry at the Mo-bound P. In contrast, intermediate **A** has a long Mo−P bond (2.44 Å) and a bent geometry at P, indicating that the P lone pair does not stabilize the 16-electron intermediate.

In the case of PEt_3, carbonyl loss from the metal results in a migration of the phosphine from the phosphinidene phosphorus to the metal, leading to the regeneration of the base-free terminal phosphinidene. Phosphine coordination to the terminal phosphinidene ligand is thus reversible, suggesting that the P−P interaction is substantially weaker than that observed in $W(CO)_5P(R)$═PEt_3. The weaker interaction indicates that the terminal phosphinidene complexes **3** and **4** are less electrophilic than the transient phosphinidene complexes $W(CO)_5PR$, as can be expected on the basis of the ancillary ligands and the amine substituents, which stabilize the base-free phosphinidene through π-donation.

Carbonyl loss from the intermediates containing a diphosphine coordinated to the phosphinidene phosphorus does not result in phosphine migration. Instead, the dangling end of the diphosphine ligand coordinates to the resulting unsaturated metal center. The resulting coordination mode, in which the diphosphines form a bridge between the metal and the phosphinidene phosphorus, is apparently stabilized by the chelate effect, since an excess of PEt_3 or PMe_3 does not result in coordination of 2 equiv of the phosphine, one to the metal and a second to phosphorus. The only exception to this reactivity pattern is in the formation of $[\{Cp^*W(CO)_2(PN(i\text{-}Pr)_2)\}_2(\mu\text{-dmpe})][AlCl_4]_2$ (**14**), in which the dmpe ligand bridges two metal centers.

The complexes $[Cp^*Mo(CO)_3\{PN(i\text{-}Pr)_2\}][AlCl_4]$ (**3**), $[Cp^*Mo(CO)_2(PEt_3)(PN(i\text{-}Pr)_2)][AlCl_4]$ (**5**), and $[Cp^*Mo(CO)(PN(i\text{-}Pr)_2)(dmpe\text{-}\kappa^2P)][AlCl_4]$ (**17**) provide a useful illustration of the effect of carbonyl for phosphine substitution on the phosphinidene ligand. The three compounds represent successive substitution of π-acceptor carbonyl ligands for strong donor phosphine ligands. For comparison, parameters for the three compounds are summarized in Table 7, along with parameters for related tungsten compounds. The M−P distances of the phosphinidene ligand follow a clear trend. As carbonyl ligands are sequentially replaced by phosphine ligands, the metal−phosphorus bond grows shorter. This change reflects the increasing electron density at the metal as π-acceptor carbonyl ligands are replaced by donor phosphine ligands. This increased electron density results in an increase in the π-back-donation from the metal to the phosphinidene, resulting in a shortening of the M−P bond. The P−N bond of the aminophosphinidene also shows a clear trend, lengthening as carbonyls are replaced by phosphines. This change is also a result of increased metal to phosphinidene π-back-donation, which reduces the amount of nitrogen to phosphorus π-donation, lengthening the P−N distance.

These trends demonstrate that the aminophosphinidene ligand acts as an effective π-acceptor ligand, given sufficient electron density at the metal. An increase in the amount of π-back-donation to the phosphinidene is expected to reduce its electrophilicity, thus altering its chemical reactivity. We are currently comparing the reactions of phosphine-substituted phosphinidene complexes such as $[Cp^*Mo(CO)_2(PEt_3)(PN(i\text{-}Pr)_2)][AlCl_4]$ (**5**) and $[Cp^*Mo(CO)(PN(i^-Pr)_2)(dmpe\text{-}\kappa^2P)][AlCl_4]$ (**17**) with those of the unsubstituted phosphinidene complexes $[Cp^*Mo(CO)_3\{PN(i\text{-}Pr)_2\}][AlCl_4]$ (**3**) and $[Cp^*W(CO)_3\{PN(i\text{-}Pr)_2\}][AlCl_4]$ (**4**) to see how different electron densities at the metal influence the reactivity at phosphorus.

Conclusion

This study has demonstrated the reactivity of stable cationic terminal molybdenum and tungsten aminophosphinidene complexes toward phosphines. These complexes are electrophilic at phosphorus, but in contrast to the well-studied transient phosphinidene complexes $W(CO)_5PR$, phosphine coordination is reversible and the P−P bond formed is weaker. Lengthening of the metal−phosphorus and phosphorus−nitrogen distances upon phosphine coordination to the phosphinidene shows that the phosphinidene acts as a π-acceptor from both the metal and the amino substituent. Phosphine substitution at the metal has been used to demonstrate that electron density at the metal significantly affects the extent of π-back-donation to the phosphinidene and indirectly affects the extent of nitrogen to phosphorus π-donation.

Experimental Section

General Comments. All procedures were carried out using standard Schlenk techniques or in a glove-box under a nitrogen atmosphere. THF was distilled from Na/benzophenone. Dichloromethane and hexane were purified using solvent purification columns containing alumina (dichloromethane) or alumina and copper oxide catalyst (hexane). Deuterated chloroform was distilled from P_2O_5 via trap-to-trap vacuum distillation. The NMR spectra were recorded at 400 or 300 MHz (^1H) and 161.975 or 121.516 MHz ($^{31}P\{^1H\}$) in $CDCl_3$, except as indicated. Infrared spectra were recorded in CH_2Cl_2 solution. The compounds $[Cp^*Mo(CO)_3\{P(Cl)N(i\text{-}Pr)_2\}]$ (**1**) and $[Cp^*W(CO)_3\{P(Cl)N(i\text{-}Pr)_2\}]$ (**2**) were prepared using the published procedures.[12,13] Triethylphosphine (PEt_3), bis(dimethylphosphino)methane (dmpm), and bis(dimethylphosphino)ethane (dmpe) were purchased from Strem and stored under nitrogen. Aluminum chloride was purified by sublimation prior to use. Elemental analyses were carried out by Guelph Chemical Laboratories. Compounds **7**, **8**, **11**, **15**, and **16** are thermally unstable intermediates and thus could not be characterized by elemental analysis.

(a) $[Cp^*Mo(CO)_2(PEt_3)(PN(i\text{-}Pr)_2)][AlCl_4]$ (5). The compound $[Cp^*Mo(CO)_3\{PN(i\text{-}Pr)_2\}][AlCl_4]$ (**3**) was prepared by dissolving

[Cp*Mo(CO)$_3${P(Cl)N(*i*-Pr)$_2$}] (**1**; 200 mg, 0.415 mmol) and $AlCl_3$ (55 mg, 0.415 mmol) in 5 mL of CH_2Cl_2. To the resulting dark red solution was added PEt_3 (49 mg, 61 μL, 0.415 mmol), resulting in a rapid color change, initially to yellow-brown and finally back to dark red. The solvent was removed in vacuo, and dark red crystals of [Cp*Mo(CO)$_2$(PEt$_3$)(PN(*i*-Pr)$_2$)][$AlCl_4$] (**5**) were grown by slow diffusion of hexanes into a CH_2Cl_2 solution. Yield: 180 mg, 61%. IR (ν(CO)): 1976, 1902 cm^{-1}. ^{31}P{^{1}H} NMR: δ 957 (d, ^2J(PP) = 15 Hz, Mo*P*N(*i*-Pr)$_2$), 36 (d, ^2J(PP) = 15 Hz, Mo*P*Et$_3$). ^{1}H NMR: δ 5.00 (sept, 1H, ^3J(HH) = 6.7 Hz, C*H*(CH$_3$)$_2$), 4.60 (bm, 1H, C*H*(CH$_3$)$_2$), 2.03 (dq, 6H, ^3J(HH) = 7.7 Hz, ^2J(HP) = 7.7 Hz, PC*H*$_2$-CH$_3$), 1.97 (s, 15H, Cp*), 1.56 (d, 6H, ^3J(HH) = 6.6 Hz, CH-(C*H*$_3$)$_2$), 1.43 (d, 6H, ^3J(HH) = 6.7 Hz, CH(C*H*$_3$)$_2$), 1.21 (dt, 9H, ^3J(HH) = 7.7 Hz, ^3J(HP) = 8.2 Hz, PCH$_2$C*H*$_3$). Anal. Calcd for $C_{24}H_{44}NO_2P_2AlCl_4Mo$: C, 40.87; H, 6.29; N, 1.99. Found: C, 40.83; H, 6.66; N, 2.00.

(b) [Cp*W(CO)$_2$(PEt$_3$)(PN(*i*-Pr)$_2$)][$AlCl_4$] (6). The compound [Cp*W(CO)$_3${P(Cl)N(*i*-Pr)$_2$}] (50 mg, 0.088 mmol) was dissolved in CH_2Cl_2 (0.6 mL), and PEt_3 (10.4 mg, 12.8 μL, 0.088 mmol) was added. There was no reaction at this point, as confirmed by ^{31}P NMR spectroscopy. The resulting solution was mixed and then added to $AlCl_3$ (12 mg, 0.09 mmol), resulting in a color change from yellow to red. The solution was transferred to a Teflon-capped sealed tube and heated to 60 °C for 1 h, resulting in a darkening of the red solution. The product was isolated as dark red crystals by slow diffusion of hexane into the CH_2Cl_2 solution. Yield: 36 mg, 62%. IR (ν(CO)): 1946, 1879 cm^{-1}. ^{31}P{^{1}H} NMR: δ 878 (b, W*P*N(*i*-Pr)$_2$), 6.2 (d, ^2J(PP) = 21 Hz, ^1J(WP) = 228 Hz, W*P*Et$_3$). ^{1}H NMR: δ 5.07 (sept, 1H, ^3J(HH) = 6.6 Hz, C*H*(CH$_3$)$_2$), 4.63 (d sept, 1H, ^3J(HH) = 6.9 Hz, ^3J(HP) <2 Hz, C*H*(CH$_3$)$_2$), 2.20 (s, 15H, Cp*), 2.05 (dq, 6H, ^3J(HH) = 7.8 Hz, ^2J(PH) = 8 Hz, PC*H*$_2$-CH$_3$), 1.54 (d, 6H, ^3J(HH) = 6.5 Hz, CH(C*H*$_3$)$_2$), 1.42 (d, 6H, ^3J(HH) = 6.6 Hz, CH(C*H*$_3$)$_2$), 1.18 (dt, 9H, ^3J(HH) = 7.8 Hz, ^3J(PH) = 16.2 Hz, PCH$_2$C*H*$_3$). Anal. Calcd for $C_{24}H_{44}NO_2P_2AlCl_4W$: C, 36.34; H, 5.59; N, 1.77. Found: C, 36.72; H, 5.88; N, 1.73.

(c) [Cp*Mo(CO)$_3${P(PEt$_3$)N(*i*-Pr)$_2$}][$AlCl_4$] (7). The compound [Cp*Mo(CO)$_3${PN(*i*-Pr)$_2$}][$AlCl_4$] (**3**) was prepared by dissolving [Cp*Mo(CO)$_3${P(Cl)N(*i*-Pr)$_2$}] (**1**; 20 mg, 0.041 mmol) and $AlCl_3$ (5.5 mg, 0.041 mmol) in 0.5 mL of CD_2Cl_2 in an NMR tube. The dark red solution was cooled to −80 °C, and triethylphosphine (5 mg, 6 μL, 0.041 mmol) was added, resulting in an immediate color change to yellow. The tube was transferred to an NMR spectrometer that had been precooled to −30 °C, and ^{31}P and ^{1}H NMR spectra were recorded. When the mixture was warmed to room temperature, evolution of gas was observed and compound **5** was formed. A similar procedure was used to record the IR spectrum in CH_2Cl_2. IR (ν(CO), −80 °C): 2013, 1947, 1917 cm^{-1}. ^{31}P{^{1}H} NMR (−30 °C, CD_2Cl_2): 78.9 (d, Mo*P*P, ^1J(PP) = 512 Hz), 32.3 (d, Mo*P*P, ^1J(PP) = 512 Hz). ^{1}H NMR (−30 °C, CD_2Cl_2): δ 3.3 (b, 2H, C*H*(CH$_3$)$_2$), 2.0 (b, 6H, PC*H*$_2$CH$_3$), 1.95 (s, 15H, C$_5$(C*H*$_3$)$_5$), 1.3 (bm, 12 H, CH(C*H*$_3$)$_2$), 1.14 (b, 9H, PCH$_2$C*H*$_3$). Compound **8** was observed using the same experimental procedure. Data for **8** are as follows. IR (ν(CO)): 2012, 1941, 1909 cm^{-1}. ^{31}P{^{1}H} NMR (−70 °C, CD_2Cl_2): 48.8 (d, W*P*P, ^1J(PP) = 503 Hz, ^1J(WP) = 116 Hz), 31.0 (d, WP*P*, ^1J(PP) = 503 Hz, ^2J(WP) = 22 Hz). ^{1}H NMR (−70 °C, CD_2Cl_2): δ 3.28 (bm, 1H, C*H*(CH$_3$)$_2$), 3.13 (bm, 1H, C*H*(CH$_3$)$_2$), 1.85−2.18 (m, 6H, PC*H*$_2$CH$_3$), 2.00 (s, 15H, C$_5$(C*H*$_3$)$_5$), 1.28 (m, 12H, CH(C*H*$_3$)$_2$), 1.06 (m, 9H, PCH$_2$C*H*$_3$).

(d) [Cp*Mo(CO)$_2${P(N(*i*-Pr)$_2$)P(Me$_2$)CH$_2$P(Me$_2$)-κ^2P^1,P^4}][$AlCl_4$] (9·[$AlCl_4$]). The compound [Cp*Mo(CO)$_3${PN(*i*-Pr)$_2$}][$AlCl_4$] (**3**) was prepared by dissolving [Cp*Mo(CO)$_3${P(Cl)N(*i*-Pr)$_2$}] (200 mg, 0.415 mmol) and $AlCl_3$ (55 mg, 0.415 mmol) in 5 mL of CH_2Cl_2. To the resulting dark red solution was added dmpm (57 mg, 67 μL, 0.415 mmol), resulting in a color change to yellow-orange and evolution of gas. The solvent was removed in vacuo, and crystals of [Cp*Mo(CO)$_2${P(N(*i*-Pr)$_2$)P(Me$_2$)CH$_2$P(Me$_2$)-κ^2P^1,P^4}][$AlCl_4$] (**9·[$AlCl_4$]**) were grown by slow diffusion of hexanes into a CH_2Cl_2 solution. Yield: 120 mg, 40%. IR (ν(CO)): 1959, 1890 cm^{-1}. ^{31}P{^{1}H} NMR: δ 109.3 (dd, ^1J(PP) = 532 Hz, ^2J(PP) = 13 Hz, Mo*P*P), 41.2 (dd, ^2J(PP) = 98 Hz, ^2J(PP) = 13 Hz, Mo*P*CH$_2$P), 10.8 (dd, ^1J(PP) = 532 Hz, ^2J(PP) = 98 Hz, MoP*P*). ^{1}H NMR: δ 3.37 (sept, 2H, ^2J(HH) = 6.6 Hz, C*H*(CH$_3$)$_2$), 2.49−2.69 (m, 2H, PC*H*$_2$P), 1.99 (dd, 3H, ^2J(HP) = 11.9 Hz, ^3J(HP) = 1.3 Hz, PP(C*H*$_3$)), 1.95 (15 H, Cp*), 1.86 (dd, 3H, ^2J(HP) = 11.5 Hz, ^3J(HP) = 3.7 Hz, PP(C*H*$_3$)), 1.78 (d, 3H, ^2J(HP) = 8.0 Hz, MoPC*H*$_3$), 1.76 (d, 3H, ^2J(HP) = 7.4 Hz, MoPC*H*$_3$), 1.18 (dd, 12H, ^2J(HH) = 6.6 Hz, ^4J(PH) = 1.6 Hz, CH(C*H*$_3$)$_2$). Anal. Calcd for $C_{23}H_{43}O_2P_3NAlCl_4Mo$: C, 38.20; H, 5.99; N, 1.94. Found: C, 37.82; H, 6.14; N, 2.08.

(e) Anion Exchange. The compound **9·[$AlCl_4$]** (50 mg, 0.069 mmol) and Na[BPh_4] (0.24 g, 0.69 mmol) were dissolved in CH_2Cl_2 (5 mL). The solvent was removed in vacuo, and the residue was extracted into toluene (20 mL) and filtered. The solution was concentrated to 5 mL, and yellow-orange crystals of [Cp*Mo(CO)$_2$-{P(N(*i*-Pr)$_2$)P(Me$_2$)CH$_2$P(Me$_2$)-κ^2P^1,P^4}][BPh_4]·C$_6$H$_5$CH$_3$ (**9·[BPh_4]**) were grown by slow evaporation. Yield: 60 mg, 99%.

(f) [Cp*W(CO)$_2${P(N(*i*-Pr)$_2$)P(Me$_2$)CH$_2$P(Me$_2$)-κ^2P^1,P^4}][$AlCl_4$] (10). The compound [Cp*W(CO)$_3${P(Cl)N(*i*-Pr)$_2$}] (50 mg, 0.088 mmol) was dissolved in CH_2Cl_2 (0.6 mL), and dmpm (11.9 mg, 13.9 μL, 0.088 mmol) was added. There was no reaction at this point, as confirmed by ^{31}P NMR spectroscopy. The solution was then added to $AlCl_3$ (12 mg, 0.09 mmol), resulting in a slight darkening of the yellow solution. This solution was then transferred to a Teflon-capped tube and monitored by ^{31}P NMR spectroscopy for 2 days, resulting in the formation of [Cp*W(CO)$_2${P(N(*i*-Pr)$_2$)P-(Me$_2$)CH$_2$P(Me$_2$)-κ^2P^1,P^4}][$AlCl_4$] (**10**). The product was isolated as orange crystals by slow diffusion of pentane into the CH_2Cl_2 solution. Yield: 43 mg, 60%. IR (ν(CO)): 1944, 1862 cm^{-1}. ^{31}P-{^{1}H} NMR: δ 91.4 (dd, ^1J(PP) = 570 Hz, ^2J(PP) = 38 Hz, ^1J(WP) = 136 Hz, W*P*P), 15.3 (dd, ^2J(PP) = 108 Hz, ^2J(PP) = 38 Hz, ^1J(WP) = 249 Hz, W*P*CH$_2$P), 14.4 (dd, ^1J(PP) = 570 Hz, ^2J(PP) = 108 Hz, ^2J(WP) = 27 Hz, WP*P*). ^{1}H NMR: δ 3.33 (m, 2H, C*H*(CH$_3$)$_2$), 2.96 (ddd, 1H, ^2J(HH) = 15 Hz, ^2J(HP) = ^2J(HP) = 11 Hz, PC*H*$_2$P), 2.55 (ddd, 1H, ^2J(HH) = 15 Hz, ^2J(HP) = 11 Hz, ^2J(HP) = 8 Hz, PC*H*$_2$P), 2.04 (s, 15 H, Cp*), 1.92 (d, 6H, ^3J(HH) = 8.1 Hz, CH(C*H*$_3$)$_2$), 1.85 (d, 6H, ^3J(HH) = 6.3 Hz, CH(C*H*$_3$)$_2$), 1.28 (b, 12H, P(C*H*$_3$)). Anal. Calcd for $C_{23}H_{43}O_2P_3NAlCl_4W$: C, 34.06; H, 5.34; N, 1.73. Found: C, 34.31; H, 5.37; N, 1.67.

(g) [Cp*Mo(CO)$_3${P(N(*i*-Pr)$_2$)P(Me$_2$)CH$_2$P(Me$_2$)-κP^1}][$AlCl_4$] (11). The compound [Cp*Mo(CO)$_3${PN(*i*-Pr)$_2$}][$AlCl_4$] was prepared by dissolving [Cp*Mo(CO)$_3${P(Cl)N(*i*-Pr)$_2$}] (20 mg, 0.041 mmol) and $AlCl_3$ (5.5 mg, 0.041 mmol) in 0.5 mL of CD_2Cl_2 in an NMR tube. The dark red solution was cooled to −80 °C, and dmpm (6 mg, 7 μL, 0.041 mmol) was added, resulting in an immediate color change to yellow. The tube was transferred to an NMR spectrometer that had been precooled to −30 °C, and ^{31}P and ^{1}H NMR spectra were recorded. When the mixture was warmed to room temperature, evolution of gas was observed and compound **9** was formed. A similar procedure was used to record the IR spectrum in CH_2Cl_2. IR (ν(CO), −80 °C): 2004, 1935, 1919 cm^{-1}. ^{31}P{^{1}H} NMR (−30 °C): δ 97.2 (d, ^1J(PP) = 506 Hz, Mo*P*P), 17.1 (dd, ^1J(PP) = 506 Hz, ^2J(PP) = 34 Hz, MoP*P*), −49.6 (d, ^2J(PP) = 34 Hz, MoPPCH$_2$*P*). ^{1}H NMR: δ 3.27 (b, 2H, C*H*(CH$_3$)$_2$), 1.96 (s, 15H, Cp*), 1.87 (bm, 2H, PC*H*$_2$P), 1.44 (d, ^1J(HH) = 6 Hz, CH-(C*H*$_3$)$_2$), 1.3 (b, 12H, P(C*H*$_3$)$_2$), 1.2 (b, 2H, CH(C*H*$_3$)$_2$).

(h)[Cp*Mo(CO)$_2${P(N(*i*-Pr)$_2$)P(Me$_2$)CH$_2$CH$_2$P(Me$_2$)-κ^2P^1,P^5}][$AlCl_4$] (12). The compound [Cp*Mo(CO)$_3${PN(*i*-Pr)$_2$}][$AlCl_4$] was prepared by dissolving [Cp*Mo(CO)$_3${P(Cl)N(*i*-Pr)$_2$}] (200 mg, 0.415 mmol) and $AlCl_3$ (55 mg, 0.415 mmol) in 5 mL of CH_2Cl_2. To the resulting dark red solution was added dmpe (62 mg, 69 μL, 0.415 mmol), resulting in a color change to yellow-orange and evolution of gas. The solvent was removed in vacuo, and crystals of [Cp*Mo(CO)$_2${P(N(*i*-Pr)$_2$)P(Me$_2$)CH$_2$CH$_2$P(Me$_2$)-κ^2P^1,P^5}][$AlCl_4$]

Table 8. X-ray Data Collection Parameters

	5	6	9	10	12	13	14	17
empirical formula	$C_{24}H_{44}AlCl_4MoNO_2P_2$	$C_{24}H_{44}AlCl_4NO_2P_2W$	$C_{54}H_{71}BMoNO_2P_3$	$C_{23}H_{43}AlCl_4NO_2P_3W$	$C_{24}H_{45}AlCl_4MoNO_2P_3$	$C_{24}H_{45}AlCl_4NO_2P_3W$	$C_{21}H_{37}AlCl_4NO_2P_2W$	$C_{23}H_{45}AlCl_4MoNOP_3$
formula wt	705.26	793.17	965.78	811.12	737.24	825.15	750.09	709.23
cryst syst	monoclinic	monoclinic	orthorhombic	monoclinic	trinclinic	triclinic	monoclinic	monoclinic
space group	$P2_1/c$	$P2_1/c$	$Pbca$	$P2_1/n$	$P\bar{1}$	$P\bar{1}$	$P2_1/c$	$P2_1/c$
unit cell dimens								
a (Å)	10.1662(5)	10.1589(5)	17.6501(9)	8.2179(5)	8.7257(4)	8.6986(9)	8.4620(8)	10.8217(7)
b (Å)	15.3421(7)	26.027(1)	16.4751(8)	14.9997(8)	12.0445(5)	12.0265(9)	14.075(1)	13.4765(9)
c (Å)	21.486(1)	12.6512(7)	35.560(2)	27.329(1)	16.6316(8)	16.658(1)	25.811(3)	23.239(1)
α (deg)	90	90	90	90	97.141(1)	96.860(2)	90	90
β (deg)	94.790(1)	94.252(1)	90	93.159(1)	98.075(1)	98.118(2)	92.33(1)	97.568(1)
γ (deg)	90	90	90	90	94.520(1)	94.601(1)	90	90
V (Å^3)	3339.5(3)	3335.9(3)	10340.5(9)	3363.6(3)	1708.91(13)	1704.4(3)	3071.6(6)	3359.7(4)
Z	4	4	8	4	2	2	4	4
calcd density (Mg m^{-3})	1.403	1.579	1.241	1.602	1.433	1.608	1.622	1.402
abs coeff (mm^{-1})	0.856	3.927	0.386	3.942	0.885	3.891	4.260	0.895
F(000)	1456	1584	4080	1616	760	824	1484	1464
θ range (deg)	1.63−28.72	1.56−28.73	1.15−28.74	1.49−28.74	1.25−28.73	1.25−28.74	1.58−28.73	1.75−28.72
index ranges	$-13 \le h \le 13$, $-20 \le k \le 20$, $-29 \le l \le 28$	$-13 \le h \le 13$, $-35 \le k \le 35$, $-17 \le l \le 17$	$-20 \le h \le 23$, $-22 \le k \le 22$, $-48 \le l \le 48$	$-11 \le h \le 11$, $-20 \le k \le 20$, $-36 \le l \le 36$	$-11 \le h \le 11$, $-16 \le k \le 16$, $-22 \le l \le 22$	$-11 \le h \le 11$, $-16 \le k \le 16$, $-22 \le l \le 22$	$-11 \le h \le 11$, $-19 \le k \le 19$, $-34 \le l \le 34$	$-14 \le h \le 14$, $-18 \le k \le 18$, $-31 \le l \le 31$
no. of rflns collected	39 404	39 320	85 889	39 442	20 439	20 223	35 984	39 425
no. of indep rflns (R(int))	8644 (0.0278)	8613 (0.0338)	13 374 (0.0517)	8661 (0.0304)	8783 (0.0261)	8726 (0.0321)	7947 (0.0380)	8693 (0.0236)
completeness to θ, %	99.9	99.7	99.7%	99.5	99.2	98.7	99.8	99.7
no. of data/restraints/params	8644/0/311	8613/0/328	13374/0/555	8661/0/316	8783/0/326	8726/0/325	7947/0/289	8693/0/320
goodness of fit on F^2	1.020	1.086	1.000	1.021	1.016	1.202	1.023	1.025
final R indices ($I > 2\sigma(I)$)								
R1	0.0238	0.0246	0.0388	0.0236	0.0367	0.0532	0.0328	0.0227
wR2	0.0591	0.0641	0.1010	0.0577	0.0918	0.1388	0.0876	0.0540
R indices (all data)								
R1	0.0295	0.0291	0.0716	0.0302	0.0517	0.0579	0.0464	0.0297
wR2	0.0619	0.0659	0.1125	0.0600	0.0978	0.1406	0.0925	0.0570
largest diff peak, hole	0.641, −0.647	0.772, −0.790	0.898, −0.735	1.528, −0.689	2.200, −0.538	3.560, −1.702	1.245, −0.500	0.804, −0.410

(**12**) were grown by slow diffusion of hexanes into a CH_2Cl_2 solution. Yield: 244 mg, 80%. IR (ν(CO), CH_2Cl_2): 1973, 1905 cm^{-1}. $^{31}P\{^1H\}$ NMR: δ 56.8 (d, $^1J(PP) = 614$ Hz, Mo*P*P), 2.3 (d, $^3J(PP) = 39$ Hz, Mo*P*CH_2CH_2P), −2.7 (dd, $^1J(PP) = 614$ Hz, $^3J(PP) = 39$ Hz, MoP*P*). ^1H NMR: δ 3.40 (bm, 2H, C*H*$(CH_3)_2$), 2.42 (bm, 2H, PC$H_2$$CH_2$P), 2.08 (bm, 2H, PC$H_2CH_2$P), 1.94 (s, 15H, Cp*), 1.69 (d, 6H, $^3J(HH) = 8$ Hz, CH(CH_3)$_2$), 1.65 (d, 6H, $^3J(HH) = 8$ Hz, CH(CH_3)$_2$), 1.19−1.16 (b, 12H, P(CH_3)$_2$). Anal. Calcd for $C_{24}H_{45}O_2P_3NAlCl_4Mo$: C, 39.10; H, 6.15; N, 1.90. Found: C, 38.57; H, 6.68; N, 1.83.

^{31}P NMR at −90 °C (CD_2Cl_2): isomer **12a**, δ 50.8 (bd, $^1J(PP) = 617$ Hz, Mo*P*P), 2.9 (dd, $^1J(PP) = 617$ Hz, $^3J(PP) = 15$ Hz, MoP*P*), 2.1 (b, Mo*P*CH_2CH_2P); isomer **12b**, δ 44.8 (d, $^1J(PP) = 623$ Hz, Mo*P*P), −1.2 (bd, $^3J(PP) = 77$ Hz, Mo*P*CH_2CH_2P), −6.8 (dd, $^1J(PP) = 623$ Hz, $^3J(PP) = 77$ Hz, MoP*P*).

(i) Reaction of [Cp*W(CO)$_3${PN(*i*-Pr)$_2$}][AlCl$_4$] (4) with dmpe. The compound [Cp*W(CO)$_3${PN(*i*-Pr)$_2$}][$AlCl_4$] was prepared by dissolving [Cp*W(CO)$_3${P(Cl)N(*i*-Pr)$_2$}] (100 mg, 0.175 mmol) and $AlCl_3$ (23 mg, 0.175 mmol) in 5 mL of CH_2Cl_2. To the resulting dark red solution was added dmpe (23 mg, 29 μL, 0.175 mmol), resulting in a color change to yellow-orange. The solvent was removed in vacuo. The ^{31}P NMR spectrum revealed a mixture of products. Two major products were isolated from the mixture by fractional crystallization and were identified as [Cp*W(CO)$_2$-{P(N(*i*-Pr)$_2$)P(Me$_2$)CH_2CH_2P(Me$_2$)-κ^2P^1,P^5}][$AlCl_4$] (**13**; yield 15 mg, 10.8%) and [{Cp*W(CO)$_2$(PN(*i*-Pr)$_2$)}$_2$(μ-dmpe)][$AlCl_4$]$_2$ (**14**; yield 22 mg, 8.38%).

(j) [Cp*W(CO)$_2${P(N(*i*-Pr)$_2$)P(Me$_2$)CH_2CH_2P(Me$_2$)-κ^2P^1,P^5}][AlCl$_4$] (13). The compound [Cp*W(CO)$_3${P(Cl)N(*i*-Pr)$_2$}] (50 mg, 0.088 mmol) was dissolved in CH_2Cl_2 (0.6 mL), and dmpe (13 mg, 14.6 μL, 0.088 mmol) was added. The resulting solution was mixed and then added to $AlCl_3$ (12 mg, 0.09 mmol), resulting in a slight darkening of the yellow solution. The solution was transferred to a Teflon-capped tube and heated to 60 °C for 1 h. The product was isolated as orange crystals by slow diffusion of pentane into the CH_2Cl_2 solution. Yield: 38 mg, 52%. IR (ν(CO), CH_2Cl_2): 1932, 1853 cm^{-1}. $^{31}P\{^1H\}$ NMR: δ 34.7 (bd, $^1J(PP) = 607$ Hz, W*P*P), −5 (bd, $^2J(PP) = 607$ Hz, WP*P*), −30 (bm, $^1J(WP) = 243$ Hz, W*P*). ^1H NMR: δ 3.4 (bm, 2H, C*H*$(CH_3)_2$), 2.44 (bm, 2H, PC$H_2$$CH_2$P), 2.22 (bm, 2H, PC$H_2$$CH_2$P), 2.03 (s, 15H, $C_5(CH_3)_5$), δ 1.71 (b, 12H, CH(CH_3)$_2$), 1.14 (b, 12H, PCH_3). Anal. Calcd for $C_{24}H_{45}NO_2P_3AlCl_4W$: C, 34.93: H, 5.50; N, 1.70. Found: C, 34.81; H, 5.78; N, 1.64.

(k) [{Cp*W(CO)$_2$(PN(*i*-Pr)$_2$)}$_2$(μ-dmpe)][AlCl$_4$]$_2$ (14). The compound [Cp*W(CO)$_3${P(Cl)N(*i*-Pr)$_2$}] (200 mg, 0.35 mmol) and $AlCl_3$ (47 mg, 0.35 mmol) were dissolved in CH_2Cl_2 (0.6 mL). The resulting dark red solution was cooled to −80 °C, and dmpe (23 μL, 26 mg, 0.17 mmol) was added, resulting in an immediate color change to orange and formation of an orange precipitate. The suspension was warmed to room temperature and stirred for 3 days, resulting in formation of a dark red solution. Addition of hexane (10 mL) resulted in the precipitation of a dark red oil, which was washed with hexane and dried under vacuum. Red-orange crystals of **14** were grown by slow diffusion of hexane into a CH_2Cl_2 solution. Yield: 52 mg, 20%. IR (ν(CO), CH_2Cl_2): 1964, 1890 cm^{-1}. $^{31}P\{^1H\}$ NMR: δ 889 (d, $^2J(PP) = 12$ Hz), −5.6 (d, $^2J(PP) = 12$ Hz, $^1J(WP) = 225$ Hz). ^1H NMR: δ 5.03 (sept, $^2J(HH) = 6.6$ Hz, 1H, C*H*$(CH_3)_2$), 4.68 (b, 1H, C*H*$(CH_3)_2$), 2.24 (s, 15H, Cp*), 2.11 (s, 6H, PCH_3), 2.08 (d, 6H, $^2J(PH) < 1$, PCH_3), 1.94 (m, 4H, PCH_2), 1.55 (d, 6H, $^2J(HH) = 6.9$ Hz, CH(CH_3)$_2$), 1.42 (d, 6H, $^2J(HH) = 6.6$ Hz, CH(CH_3)$_2$). Anal. Calcd for $C_{42}H_{74}N_2O_4P_4$-$Al_2Cl_8W_2$: C, 33.63: H, 4.97; N, 1.87. Found: C, 33.21; H, 4.78; N, 1.79.

(l) [Cp*W(CO)$_2${P(N(*i*-Pr)$_2$)P(Me$_2$)CH_2CH_2P(Me$_2$)-κP^1}][AlCl$_4$] (15). The compound [Cp*W(CO)$_3${PN(*i*-Pr)$_2$}][$AlCl_4$] was prepared by dissolving [Cp*W(CO)$_3${P(Cl)N(*i*-Pr)$_2$}] (30 mg, 0.053 mmol) and $AlCl_3$ (7.1 mg, 0.053 mmol) in CD_2Cl_2 (0.5 mL). The solution was cooled to −80 °C, and dmpe (8.8 μL, 8.0 mg, 0.053 mmol) was added, resulting in a color change from red-orange to yellow. The solution was transferred to an NMR tube at −80 °C, and the ^{31}P and ^1H NMR spectra were recorded at −80 °C. $^{31}P\{^1H\}$ NMR (−80 °C, CD_2Cl_2): δ 52.9 (d, $^1J(PP) = 493$ Hz, $^1J(WP) = 113$ Hz, W*P*), 17.8 (dd, $^1J(PP) = 493$ Hz, $^3J(PP) = 33$ Hz, WP*P*), −42.2 (d, $^3J(PP) = 33$ Hz, WPCH_2CH_2*P*). ^1H NMR (−80 °C, CD_2Cl_2): δ 3.19 (bm, 2H, NC*H*$(CH_3)_2$), 2.1 (bm, 2H, PP$CH_2$$CH_2$P), 2.0 (s, 15H, Cp*), 1.6 (d, 6H, NCH(CH_3)$_2$), 1.4 (bm, 2H, PPCH_2CH_2P), 1.23 (d, 6H, NCH(CH_3)$_2$), 1.09 (s, 6H, PCH_3), 0.99 (s, 6H, PCH_3).

(m) [{Cp*W(CO)$_2$}$_2$(μ-P(N(*i*-Pr)$_2$)P(CH$_3$)$_2$CH$_2$CH$_2$P(CH$_3$)$_2$P-(N(*i*-Pr)$_2$))][AlCl$_4$]$_2$ (16). The compound [Cp*W(CO)$_3${PN(*i*-Pr)$_2$}]-[$AlCl_4$] was prepared by dissolving [Cp*W(CO)$_3${P(Cl)N(*i*-Pr)$_2$}] (30 mg, 0.053 mmol) and $AlCl_3$ (7.1 mg, 0.053 mmol) in CD_2Cl_2 (0.5 mL). The solution was cooled to −80 °C and dmpe (3.5 μL, 3.1 mg, 0.021 mmol) was added, resulting in a color change from red-orange to yellow. The solution was transferred to an NMR tube at −80 °C, and the ^{31}P and ^1H NMR spectra were recorded at −80 °C. $^{31}P\{^1H\}$ NMR (−80 °C): δ 58 (b), 17.9 (d, $^1J(PP) = 523$ Hz). ^1H NMR (−80 °C): δ 3.1 (b, 2H, NC*H*$(CH_3)_2$), 2.2 (bm, 4H, PCH_2CH_2P), 2.0 (s, 15H, Cp*), 1.4 (b, 12H, NCH(CH_3)$_2$), 1.1 (b, 12H, PCH_3).

(n) [Cp*Mo(CO)(PN(*i*-Pr)$_2$)(dmpe-κ^2P)][AlCl$_4$] (17). The compound [Cp*Mo(CO)$_2${P(N(*i*-Pr)$_2$)P(Me$_2$)CH_2CH_2P(Me$_2$)}][$AlCl_4$] (**12**; 100 mg, 0.135 mmol) was dissolved in THF (20 mL) and irradiated for 2 h (mercury vapor lamp, Pyrex cutoff), resulting in a color change to dark orange-brown. The solvent was removed in vacuo and the residue extracted into CH_2Cl_2 (1 mL). Dark orange crystals of [Cp*Mo(CO)(PN(*i*-Pr)$_2$)(dmpe-κ^2P)][$AlCl_4$] (**17**) were grown by slow diffusion of hexane into the CH_2Cl_2 solution. Yield: 12 mg, 12.6%. IR (ν(CO), CH_2Cl_2): 1883 cm^{-1}. $^{31}P\{^1H\}$ NMR: δ 1057.7 (b), 52.99 (dd, $^2J(PP) = 37$ Hz, $^2J(PP) = 11$ Hz), 44.87 (dd, $^2J(PP) = 37$ Hz, $^2J(PP) = 13$ Hz). ^1H NMR: δ 4.6 (sept, 1H, $^3J(HH) = 8.4$ Hz, C*H*$(CH_3)_2$), 4.5 (bm, 1H, C*H*$(CH_3)_2$), 2.01 (s, 15H, Cp*), 1.79 (d, 6H, $^3J(HH) = 8.4$ Hz, CH(CH_3)$_2$), 1.54 (d, 6H, $^3J(HH) = 8.4$ Hz, CH(CH_3)$_2$), 1.45 (m, 4H, PCH_2CH_2P), 1.29 (s, 12H, P(CH_3)$_2$). Anal. Calcd for $C_{24}H_{44}NO_2P_2$-$AlCl_4W$: C, 38.95; H, 6.39; N, 1.97. Found: C, 38.42; H, 6.09; N, 1.85.

Computational Studies. Calculations were carried out using Gaussian 03[25] using B3LYP and a mixed basis set: LanL2DZ for Mo and 6-31G* for light atoms. Geometries were optimized and energies were calculated for [Cp*Mo(CO)$_3${PN(*i*-Pr)$_2$}]$^+$ (**3**) and [Cp*Mo(CO)$_3${P(Et$_3$)N(*i*-Pr)$_2$}]$^+$ (**7**) and for the proposed intermediates that result from carbonyl loss from **3** and **7**, [Cp*Mo-(CO)$_2${PN(*i*-Pr)$_2$}]$^+$ (**A**) and [Cp*Mo(CO)$_2${P(PEt$_3$)N(*i*-Pr)$_2$}]$^+$ (**B**). The ΔE value for carbonyl loss was calculated by subtracting energies of **3** or **7** from the energies of the dicarbonyl intermediates and CO. Optimized energies are given in Table 9. Conformers of [Cp*Mo(CO)$_2${P(N(*i*-Pr)$_2$)P(Me$_2$)CH_2CH_2P(Me$_2$)-κ^2P^1,P^5}]-[$AlCl_4$] (**12**) were optimized using the same method and basis set. Two minima, which correspond to chair and boat conformations of the six-membered MPPCCP ring, were identified.

(25) Frisch, M. J.; Trucks, G. W.; Schlegel, H. B.; Scuseria, G. E.; Robb, M. A.; Cheeseman, J. R.; Montgomery, J. A., Jr.; Vreven, T.; Kudin, K. N.; Burant, J. C.; Millam, J. M.; Iyengar, S. S.; Tomasi, J.; Barone, V.; Mennucci, B.; Cossi, M.; Scalmani, G.; Rega, N.; Petersson, G. A.; Nakatsuji, H.; Hada, M.; Ehara, M.; Toyota, K.; Fukuda, R.; Hasegawa, J.; Ishida, M.; Nakajima, T.; Honda, Y.; Kitao, O.; Nakai, H.; Klene, M.; Li, X.; Knox, J. E.; Hratchian, H. P.; Cross, J. B.; Bakken, V.; Adamo, C.; Jaramillo, J.; Gomperts, R.; Stratmann, R. E.; Yazyev, O.; Austin, A. J.; Cammi, R.; Pomelli, C.; Ochterski, J. W.; Ayala, P. Y.; Morokuma, K.; Voth, G. A.; Salvador, P.; Dannenberg, J. J.; Zakrzewski, V. G.; Dapprich, S.; Daniels, A. D.; Strain, M. C.; Farkas, O.; Malick, D. K.; Rabuck, A. D.; Raghavachari, K.; Foresman, J. B.; Ortiz, J. V.; Cui, Q.; Baboul, A. G.; Clifford, S.; Cioslowski, J.; Stefanov, B. B.; Liu, G.; Liashenko, A.; Piskorz, P.; Komaromi, I.; Martin, R. L.; Fox, D. J.; Keith, T.; Al-Laham, M. A.; Peng, C. Y.; Nanayakkara, A.; Challacombe, M.; Gill, P. M. W.; Johnson, B.; Chen, W.; Wong, M. W.; Gonzalez, C.; Pople, J. A. *Gaussian 03*, revision C.02; Gaussian, Inc.: Wallingford, CT, 2004.

Table 9. Optimized Energies

compd	energy (kJ/mol)
3	−214 570.190 9
7	−301 412.752 7
A	−197 567.613 6
B	−284 413.689 3
CO	−16 993.967 26

X-ray Analyses. Suitable crystals of compounds **5**, **6**, **9**, **10**, **12**−**14**, and **17** were mounted on glass fibers. Diffraction measurements were made on a Siemens SMART CCD automatic diffractometer using graphite-monochromated Mo Kα radiation. Unit cells were determined from randomly selected reflections obtained using the SMART CCD automatic search, center, index, and least-squares routines. Integrations were carried out using the program SAINT, and absorption corrections were performed using SADABS. Structure solutions were carried out using the SHELXTL 5.1 suite of programs. The initial solutions were obtained by direct methods and refined by successive least-squares cycles. Data collection and structure solution parameters are given in Table 8.

Acknowledgment. This work was supported by the National Research Council of Canada, by the University of Regina, and by grants from the Natural Sciences and Engineering Research Council of Canada (to A.J.C. and B.T.S.) and NRC-NSERC Canadian Government Laboratories Visiting Fellowships (to B.T.S. and O.S.S.). B.T.S. wishes to acknowledge Dr. Lynn Mihichuk for helpful discussions.

Supporting Information Available: Crystallographic data for compounds **5**, **6**, **9**, **10**, **12**−**14**, and **17** (CIF files) and optimized structures for **3**, **7**, **A**, and **B** (mol2 format). This material is available free of charge via the Internet at http://pubs.acs.org.

OM060685X